

THE EFFECT OF BEAM PARAMETERS ON VORTEX BEAMS
PROPAGATING IN ATMOSPHERIC TURBULENCE

A THESIS SUBMITTED TO
THE GRADUATE SCHOOL OF NATURAL AND APPLIED SCIENCES

OF
ÇANKAYA UNIVERSITY

BY

KHOLOUD ELMABRUK

IN PARTIAL FULFILLMENT OF THE REQUIREMENTS
FOR
THE DEGREE OF DOCTOR OF PHILOSOPHY
IN
ELECTRONIC AND COMMUNICATION ENGINEERING

JANUARY 2020

Title of the Thesis: **The Effect of Beam Parameters on Vortex Beams Propagating in Atmospheric Turbulence**

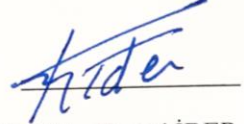
Submitted by **Kholoud ELMABRUK**

Approval of the Graduate School of Natural and Applied Sciences, Çankaya University.



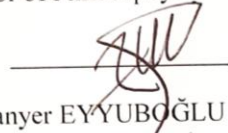
Prof. Dr. Can ÇOĞUN
Director

I certify that this thesis satisfies all the requirements as a thesis for the degree of Doctor of Philosophy.



Prof. Dr. Sitki Kemal İDER
Head of Department

This is to certify that we have read this thesis and that in our opinion it is fully adequate, in scope and quality, as a thesis for the degree of Doctor of Philosophy.

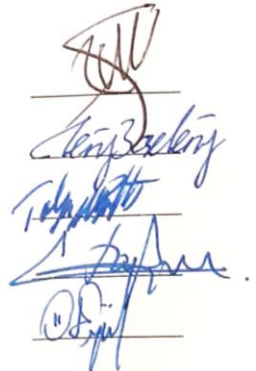


Prof. Dr. Halil Tanyer EYYUBOĞLU
Supervisor

Examination Date: 28.01.2020

Examining Committee Members

Prof. Dr. Halil Tanyer EYYUBOĞLU	(Çankırı Karatekin Univ.)
Assoc. Prof. Dr. H. Deniz BAŞDEMİR	(Çankaya Univ.)
Assoc. Prof. Dr. Tolga PUSATLI	(Çankaya Univ.)
Prof. Dr. M. Cengiz TAPLAMACIOĞLU	(Gazi Univ.)
Asst. Prof. Dr. Özgür ERGÜL	(Atılım Univ.)



STATEMENT OF NON-PLAGIARISM PAGE

I hereby declare that all information in this document has been obtained and presented in accordance with academic rules and ethical conduct. I also declare that, as required by these rules and conduct, I have fully cited and referenced all material and results that are not original to this work.

Name, Last Name: Kholoud ELMABRUK

Signature:



Date: 28.01.2020

ABSTRACT

THE EFFECT OF BEAM PARAMETERS ON VORTEX BEAMS PROPAGATING IN ATMOSPHERIC TURBULENCE

ELMABRUK, Kholoud

Ph.D., Electronic and Communication Engineering Department

Supervisor: Prof. Dr. Halil Tanyer EYYUBOĞLU

January 2020, 65 pages

The effect of beam parameters on the intensity profile of vortex beams propagating in the turbulent atmosphere and the scintillation properties of these beams are analyzed. A random phase screen model is utilized to perform this analysis. The scintillation properties are evaluated against the changes of topological charge, beam order, operating wavelength, receiver aperture side length, and source size parameters. The results show that using a flat-topped Gaussian vortex beam with a high topological charge causes a reduction in scintillation. Increasing the receiver aperture side length reduces the scintillation level. As the source size increases, scintillation decreases. The presented results also indicate that a flat-topped Gaussian vortex beam with high topological charges has less scintillation than the fundamental Gaussian beam.

Moreover, the beams with higher topological charges and the ones operating at higher wavelengths preserve their beam profile better as they propagate. The beam order does not affect the beam profile. As the source size of the beam increases the intensity profile experiences dramatic changes concerning the beam propagating in free space. The findings of this dissertation will be useful in improving the performance of next-generation optical communication links and networks.

Keywords: Flat-topped Gaussian vortex beam; Bessel Gaussian vortex beam; Topological charge; operating wavelength; source size; scintillation; random phase screen; turbulence.

ÖZ

HÜZME PARAMETRELERİNİN ATMOSFERİK TÜRBÜLANSTA YAYILAN VORTEKS HÜZMELERİ ÜZERİNDEKİ ETKİSİ

ELMABRUK, Kholoud

Doktora, Elektronik ve Haberleşme Mühendisliği Bölümü

Danışman: Prof. Dr. Halil Tanyer EYYUBOĞLU

Ocak 2020, 65 sayfa

Hüzme parametrelerinin türbülanslı atmosferde yayılan girdap hüzmelerinin yoğunluk profili üzerindeki etkisi ve bu hüzmelerin sintilasyon özellikleri analiz edilir. Bu analizi gerçekleştirmek için rastgele bir faz tarama modeli kullanılmıştır. Sintilasyon özellikleri topolojik yük, ışın sırası, çalışma dalga boyu, alıcı diyafram tarafı uzunluğu ve kaynak boyutu parametrelerindeki değişikliklere göre değerlendirilir. Sonuçlar, yüksek topolojik yüke sahip düz tepeli bir Gauss vorteks ışınının kullanılmasının sintilasyonda bir azalmaya neden olduğunu göstermektedir. Alıcı açıklığı yan uzunluğunun arttırılması, sintilasyon seviyesini azaltır. Kaynak boyutu arttıkça sintilasyon azalır. Sunulan sonuçlar ayrıca yüksek topolojik yüklere sahip düz tepeli bir Gauss vorteks ışınının temel Gauss ışına göre daha az sintilasyona sahip olduğunu göstermektedir.

Ayrıca, daha yüksek topolojik yükleri olan ışınlar ve daha yüksek dalga boylarında çalışan ışınlar, yayıldıkça ışın profillerini korurlar. Işın sırası, ışın profilini etkilemez. Hüzme kaynak boyutu arttıkça, ışın profili dramatik değişiklikler yaşar. Bu tezin bulguları, yeni nesil optik iletişim bağlantılarının ve ağlarının performansının iyileştirilmesinde faydalı olacaktır.

Anahtar Kelimeler: Düz tepeli Gauss girdap demeti; Bessel Gauss girdap demeti; Topolojik yük; dalga boyu; kaynak boyutu; sintilasyon; rastgele faz ekranı; türbülans.

ACKNOWLEDGMENTS

First, I would like to express my sincere gratitude to my advisor, Professor Halil Tanyer EYYUBOĞLU for his patience, time, and continuous support that made my steps in the field stronger and much easier.

I am indebted to my family, primarily my father and mother for everything. My deepest appreciation belongs to my husband and my sons for their patience on all my stresses, I am truly thankful for their support and generous love. I should also thank my sisters for their continuous support and encouragement in each step in my Ph.D...

2020, 28 January

Kholoud Elmabruk

TABLE OF CONTENTS

STATEMENT OF NON-PLAGIARISM PAGE	iii
ABSTRACT	iv
ÖZ	v
TABLE OF CONTENTS	vii
LIST OF FIGURES	ix
LIST OF TABLES	xi
LIST OF ABBREVIATIONS	xii
CHAPTER 1	1
Introduction	1
1.1 Background	1
1.2 Free Space Optical Communication	3
1.2.1 FSO communication link	3
1.2.2 FSO Communication Link Limitations	4
1.3 Orbital Angular Momentum Beams	6
1.3.1 Historical Background.....	6
1.3.2 OAM Beams Advantages and Applications	7
1.4 Research Motivations and Objectives.....	7
1.5 Thesis Organization	9
CHAPTER 2.....	10
Beam Propagation through Random Medium.....	10
2.1 Atmosphere	10
2.2 Atmospheric Turbulence.....	11

2.3	Weak and Strong Turbulence Conditions	12
2.4	Power Spectrum Models for Optical Turbulence	12
2.6	Propagation of Vortex Beams in a Turbulent Atmosphere	14
CHAPTER 3		16
Propagation of Vortex Beams in Atmosphere.....		16
3.1	Introduction	16
3.2	Turbulence Modeling.....	17
3.3	Scintillation Expressions.....	19
3.4	Constructing the Random Phase Screen Model	20
3.5	Vortex Beams under Consideration.....	21
CHAPTER 4.....		24
Effect of Beam Parameters on Vortex Beams Propagating in Atmospheric Turbulence.....		24
4.1	Random Phase Screens Design	24
4.2	Flat-topped Gaussian Vortex Beam.....	25
4.3	Bessel Gaussian Vortex Beam	30
CHAPTER 5.....		35
Effect of Beam Parameters on the Scintillation Properties of Vortex Beams.....		35
5.1	Random Phase Screens Model	35
5.2	Scintillation Properties of Flat-topped Gaussian Vortex Beam	37
CHAPTER 6.....		42
Conclusion.....		42
References		44

LIST OF FIGURES

Figure 1.1 Optical wireless communication applications	2
Figure 1.2 Categories of optical wireless communication	2
Figure 1.3 FSO Applications	3
Figure 1.4 Block diagram of the FSO communication links	4
Figure 1.5 Atmospheric Effects	5
Figure 1.6 (a) linearly polarized light without SAM, (b) circularly polarized light with SAM of $\pm\hbar$ per photon [15]	6
Figure 2.1 Atmospheric Layers	10
Figure 2.2 Propagation of optical beams in atmospheric turbulence	11
Figure 2.3 The Kolmogorov cascade theory of turbulence	12
Figure 3.1 The spatial profile, phase and wavefront of vortex beam vs. Gaussian beam	17
Figure 3.2 Flat-topped Gaussian vortex beam in the source plane (a, b) $m = 1, N = 1$, (c, d) $m = 5, N = 1$	22
Figure 3.3 Bessel Gaussian vortex beam in the source plane (a, b) $m = 1$, (c, d) $m = 5$	23
Figure 4.1 Received normalized average intensity of flat-topped Gaussian vortex beam propagating in turbulence at different topological charges (m)	26
Figure 4.2 Received normalized average intensity of flat-topped Gaussian vortex beam propagating in turbulence at different beam orders (N)	27
Figure 4.3 Received normalized average intensity of flat-topped Gaussian vortex beam propagating in turbulence at different propagation distances (L)	28
Figure 4.4 Received normalized average intensity of flat-topped Gaussian vortex beam propagating in turbulence at different source sizes (α_s)	29
Figure 4.5 Received normalized average intensity of flat-topped Gaussian vortex beam propagating in turbulence at different operating wavelength (λ)	30
Figure 4.6 Received normalized average intensity of Bessel Gaussian vortex beam propagating in turbulence at different topological charges (m)	31
Figure 4.7 Received normalized average intensity of Bessel Gaussian vortex beam propagating in turbulence at different propagation distances (L)	32
Figure 4.8 Received normalized average intensity of Bessel Gaussian vortex beam propagating in turbulence at different source sizes (α_s)	33
Figure 4.9 Received normalized average intensity of Bessel Gaussian vortex beam propagating in turbulence at different operating wavelength (λ)	34

Figure 5.1 The receiver aperture side length variation versus the propagation distance	36
Figure 5.2 Comparing the scintillation of flat-topped Gaussian vortex beam from random phase screen model and analytic formulation	36
Figure 5.3 The effect of changing the topological charge on the scintillation properties of flat-topped Gaussian vortex beam	37
Figure 5.4 The effect of changing the beam order on the scintillation properties of flat-topped Gaussian vortex beam	38
Figure 5.5 The effect of changing the source size on the scintillation properties of flat-topped Gaussian vortex beam	39
Figure 5.6 The effect of changing the side length of receiver aperture on the scintillation properties of flat-topped Gaussian vortex beam	39
Figure 5.7 The effect of changing the operating wavelength on the scintillation properties of flat-topped Gaussian vortex beam	40
Figure 5.8 Comparing the scintillation properties of flat-topped Gaussian vortex beam with the Gaussian beam	41

LIST OF TABLES

Table 3.1 The turbulence strength of the studied cases.....	20
--	----



LIST OF ABBREVIATIONS

OWC	Optical Wireless Communication
IR	Infrared
VL	Visible
LOS	Line Of Sight
FSO	Free-space Optical Communication systems
IM	Intensity Modulation
LED	Light-Emitting Diodes
BER	Bit Error Rate
OAM	Orbital Angular Momentum
SAM	Spin Angular Momentum
FT	Flat-Topped beams

NOMENCLATURE

\hbar	Planck's constant
θ	Azimuthal coordinate in the beam's cross-section
m	Topological charge
r	Radial coordinate
L_n^m	Laguerre polynomial
L_0	Outer scale of turbulence
l_0	Inner scale of turbulence
C_n^2	Refractive index structure constant
k	Wave number
λ	Operating wavelength
L	Propagation distance
σ_R^2	Rytov variance
R	Distance separating between two points
κ	Scalar wave number
s	Source plane transverse coordinates
$u_s(s_x, s_y)$	Source field
$u_{rfs}(\mathbf{r}, L)$	Free space received field
$h(r)$	Transfer function
F	Fourier transform operator
F^{-1}	Inverse transform
\mathbf{f}	Spatial frequency
$\emptyset(\mathbf{r})$	Phase power spectral density of the individual screens of random phase distribution
$I_r(\mathbf{r}, L)$	Intensity of the received field
$b^2(\mathbf{r}, L)$	Scintillation index
$P_r(L)$	Received beam instantaneous power over a squared aperture
L_a	Receiver side length

α_s Source size
 N Beam order



CHAPTER 1

Introduction

1.1 Background

The use of the atmosphere as a transmission medium was employed for the first time in 1880 by Alexander Graham Bell, in the experiment so-called "photophone" in which he transmitted the human voice signals to an optical receiver at a distance of few hundreds of meters through sunlight [1, 2]. Although this experiment was performed without the use of lasers it was a milestone in optical communications. Then, the significant improvement in lasers, optoelectronic devices, and optical detectors made the applications of optical communications an essential part of our daily life.

In optical wireless communication (OWC) systems the information is transferred from one point to another using optical carrier [3]. OWC has improved rapidly and has achieved great advantages over the other communication systems. OWC systems can be considered as an attractive technology for high-speed broadband systems due to their abilities to offer extremely high bandwidth, easing of deployment, improving the channel security, reducing the power consumption, and their unlicensed spectrum allocation [4]. OWC has an enormous range of applications as shown in Figure 1.1, some of the crucial applications are mobile phones, tablets, portable media players, radios, televisions, wireless remote devices, several communication protocols, robotics, smart cars, smart Grid, biomedical devices, satellites, radars and astronomy, industry, healthcare...etc. [3, 4].

There are two main categories of the OWC, namely the indoor and outdoor OWC. The indoor OWC utilizes infrared (IR) or visible light (VL) as a carrier to communicate. It plays a great role in the in-building wireless applications especially in cases where the wired networks become challenging. Indoor OWC can be further classified into four groups namely, non-directed line of sight (LOS), directed LOS

tracked and diffused. The outdoor OWC transports information through the unguided channel (either atmosphere or free-space). Accordingly, outdoor OWC technology is known as the co-called free-space optical communication systems (FSO). The FSO systems are divided up to terrestrial links and space optical links that are mainly divided into building-to-building, ground-to-satellite, satellite-to-ground, and satellite-to-satellite [5-7].



Figure 1.1 Optical wireless communication applications

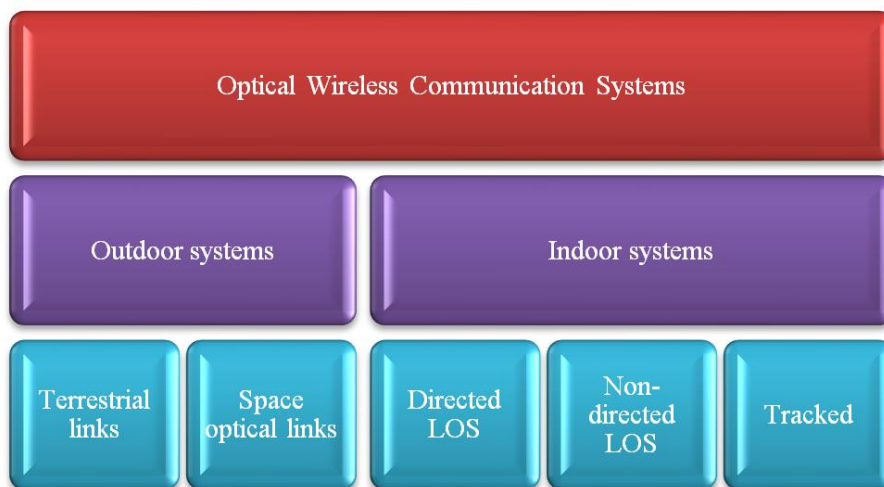


Figure 1.2 Categories of optical wireless communication

1.2 Free Space Optical Communication

FSO communication systems have recently become an important technology in a tremendous range of applications due to their attractive properties. Its large bandwidth, high data rate, less power, and low mass requirements emerged as a new technology for many applications like in the military, remote sensing, disaster recovery, radio astronomy, and wireless cellular networks, etc. as illustrated in Figure 1.3 [6]. FSO communication transfer data from point to another employing an optical carrier in the near IR band.

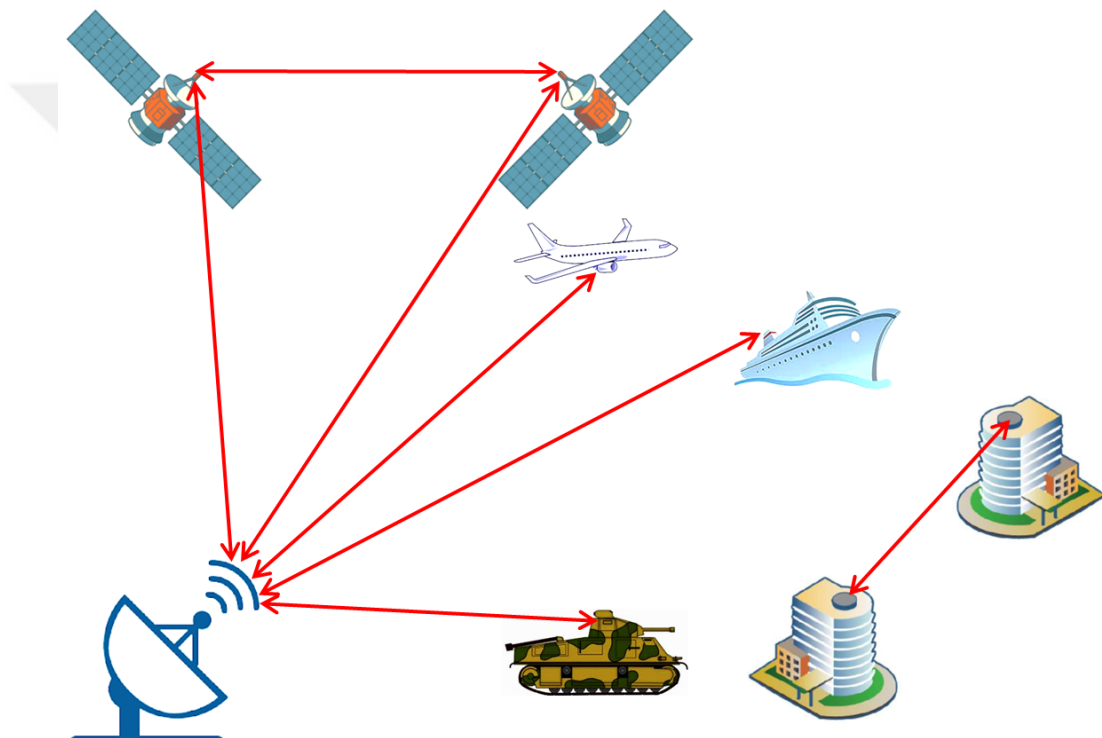


Figure 1.3 FSO Applications

1.2.1 FSO Communication Link

Like any of the other communication systems, a typical FSO system consists of three main parts namely, the transmitter, the receiver and the channel as demonstrated in Figure 1.4.

Transmitter: is the part of the system that is responsible for the modulation of the source data on the optical carrier that will propagate during the channel towards the receiver. Intensity modulation (IM) is a widely used modulation technique where the

message signal is modulated on the optical carrier intensity. Then, the telescope collects, collimates and directs the modulated optical carrier towards the receiver. Light-emitting diodes (LED) and LASERs are the most commonly used optical sources in FSO systems [6, 7].

Channel: FSO communication systems utilize the atmosphere as the propagation medium of the transmitted signals. Many unforeseeable environmental factors (fog, snow, rain, wind, and clouds) affect the FSO channel. Since these factors have changeable characteristics that cause the received signal to be attenuated and deteriorated [6, 7].

Receiver: is the part of the system that is responsible for detecting the message signal from the received signal. In the FSO system, the receiver consists of four main units namely the telescope, optical filter, photodetector and the decision unit “detection circuit”. The telescope collects the incident optical signal then focuses it on the optical filter which reduces the background radiation and allows only the operating wavelengths to pass to the photodetector. The photodetector is responsible for converting the coming optical signal to an electrical signal which will be amplified and sent to the decision unit where the signal will be covered [6, 7].

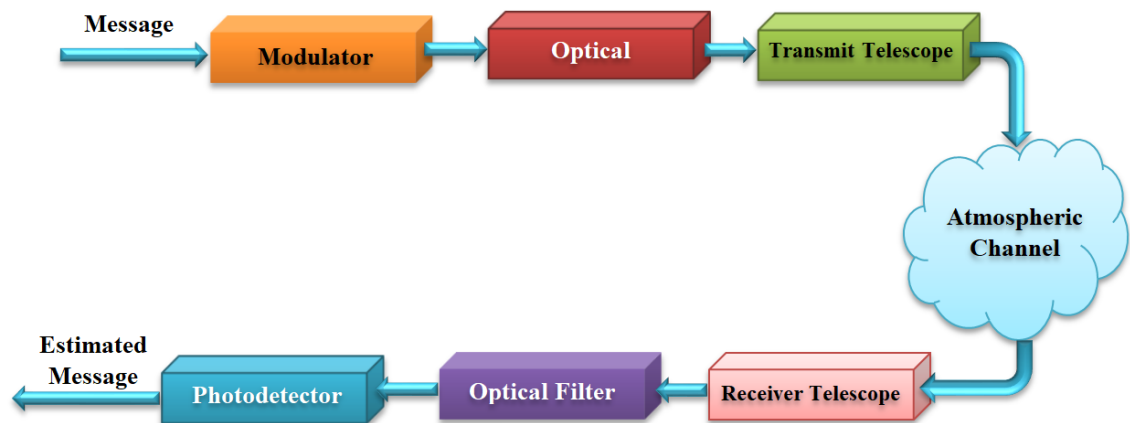


Figure 1.4 Block diagram of the FSO communication links

1.2.2 FSO Communication Link Limitations

Although the FSO systems have great advantages, the use of the atmosphere as a propagating medium limits the performance of these systems. In these systems, the dependency on the weather and geographical location addresses strong limitations on

the signals propagating that depredate the bit error rate (BER) performance of the FSO link. The system performance is affected mostly by the scattering, absorption, and turbulence [7-9].

1.2.2.1 Atmospheric Effects

The atmospheric conditions variations can be caused by different factors such as rain, snow, wind, haze, etc., which affect the optical beams propagating in the FSO links. In these links, there are three main atmospheric phenomena (namely, absorption, scattering, and turbulence) that affect the optical beams as illustrated in Figure 1.5.

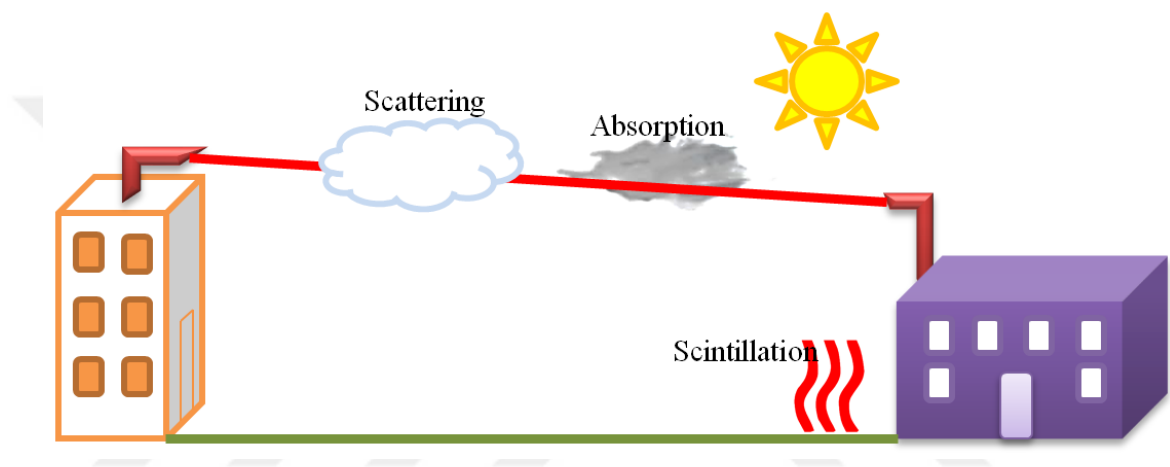


Figure 1.5 Atmospheric Effects

In the atmosphere, the constituent gas and particles attenuate the energy of the propagating light beam by the absorption and scattering phenomena. Absorption occurs when a gaseous molecule absorbs a photon of the propagating light and converts it into kinetic energy. Scattering occurs when the propagating light beam collides with air molecules and particles. This phenomenon is wavelength-dependent [7]. The difference between the Earth's surface and the atmosphere temperature causes refractive index fluctuations which refer to as turbulence. The turbulence has a strong impact on the FSO link performance, therefore it is important to investigate its effect on the propagation of the light beam.

1.3 Orbital Angular Momentum Beams

1.3.1 Historical Background

Light has mechanical properties when considered as a wave. Accordingly, since light beams carry linear momentum, the comet tails are always pointing away from the sun as Kepler proposed. In 1905, John Poynting evolved the theory of electromagnetic radiation momentum density [10]. Then in 1909, Poynting recognized that circularly polarized light has a spin angular momentum with a value of $\pm\hbar$ per a single photon ($\hbar = h/2\pi$ where h is Planck's constant). Moreover, he stated that any polarization state conversion is to be followed by an angular momentum exchange [11]. In 1936, Beth demonstrated the polarization transfer between polarized light and the rotational motion of a birefringent wave plate hanged on a filament [12]. In the 1950s scientists realized for the higher-order transitions to occur the generated light has to carry multiple units of angular momentum \hbar so orbital angular momentum (OAM) besides the spin. Moreover, scientists recognized that linearly polarized light carries linear momentum with $\hbar k_0$ per photon; on the other hand, circularly polarized light carries a spin angular momentum (SAM) of $\pm\hbar$ per photon [10]. Allen et al. in 1992 realized that light beams carry OAM when they have an azimuthal phase dependency of $\exp(\pm im\theta)$ (where θ is the azimuthal coordinate in the beam's cross-section m is any positive or negative integer known as the topological charge) [13]. The OAM is the component of the angular momentum which depends on the spatial field distribution and irrelevant to the polarization, it also appears as a circular polarization and associated with the photon spin; moreover, it is completely different than the SAM as illustrated in **Error! Reference source not found.** Each of OAM and SAM can be derived from Maxwell's equations [10, 14-17].

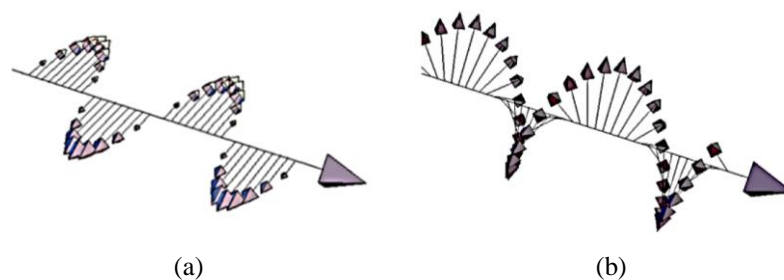


Figure 1.6 (a) linearly polarized light without SAM, (b) circularly polarized light with SAM of $\pm\hbar$ per photon [15]

Beams with OAM are spatially structured with helical phase fronts. These beams can be generated with computer-generated hologram, spatial light modulated, phase plates and also using constructing lasers that emit helical Laguerre-Gaussian modes. The azimuthal helical wave function of these modes is [18]:

$$\psi_{LG}(r, \theta) \propto L_n^m(r) e^{il\theta} \quad (1.1)$$

where, r is the radial coordinate and L_n^m is the Laguerre polynomial with n being the degree of the polynomial.

1.3.2 OAM Beams Advantages and Applications

Orbital angular momentum beams (OAM) are a technology with a new fundamental degree of freedom that has revolutionised great diversity in a wide range of applications. These beams have emerged in optical manipulation, biomedical applications, micro-fabrication, super-resolution microscopy, imaging, trapping and tweezers in biosciences and micro-mechanics and also in the new generation of optical communication [15-22].

In these applications, the use of OAM beams is due to their unique properties. The control of the beam's OAM is critical since in optical manipulation the rotation speed of the trapped microparticle depends on the state of the OAM. OAM beams offer a large capacity and high dimensional information processing in optical communications due to the multiple obtainable OAM states. In free-space links, the spatial generated OAM beams using namely spiral phase plates, computer-generated fork holograms, spatial light modulators, and cylindrical lens pairs have low crosstalk and strong scalability [17].

1.4 Research Motivations and Objectives

Nowadays, regarding the increasing demand for larger bandwidth and higher data rates, FSO communications in a diversity of applications such as 5G and 6G

communication links, laser satellite communications, and remote sensing have achieved rapid growth and development. In these applications, the propagation of the laser beam in the atmosphere (channel) degrades the probability of error performance of the system due to the atmospheric effects [7].

Moreover, a tremendous number of studies focused on the examination of the physical properties of light namely, amplitude, phase, and polarization to achieve the required higher data rates. Recently, the rotation of the propagating beam became one of the most important properties of the light beams. The light beam spins when every polarized vector rotates, but the light beam has OAM when phase structure rotates. The OAM (vortex) beams became very promising for the FSO communications since their phase distribution can be modulated to transmit the message signal. Thus, these beams propose an alternative to the classical intensity or phase modulations that FSO communication links use [23].

The essential aim of this thesis is to estimate the expediency of vortex beams for short and medium range optical communication links. Accordingly, this dissertation targets to search the suitability of vortex beams in FSO systems through investigating the effect of beam parameters (topological charge, beam order, propagation distance, operating wavelength and source size) on the vortex beams propagating in turbulent atmosphere. The main contributions of this thesis are:

- Investigating the effect of the beam parameters on the received intensity of the vortex beams that travelled a distance in atmospheric turbulence. This analysis will help to improve the system performance. To ensure the obtained results reliability we compare them with the analytical findings.
- Providing a detailed analysis of the scintillation properties of the vortex beams propagating in turbulent atmosphere. The effect of source beam, propagation and receiver plane parameters on scintillation reduction of the vortex beams is obtained and compared with the analytical models in literature.

1.5 Thesis Organization

The dissertation is organized in six chapters. Chapter 2 covers the background of light beams propagation in a random medium. Chapter 3 involves the theoretical representation of vortex beams propagation in atmospheric turbulence. Moreover, it presents the random phase screen design and results. Chapter 4 studies the effect of beam parameters on the intensity profile of vortex beams propagating in turbulent atmosphere. Chapter 5 analyses the effect of beam parameters on the scintillation properties of vortex beams propagating in turbulent atmosphere. Finally, chapter 6 summarizes the presented work and highlights the main contributions. Subsequently, presents the suggestions for the future research.



CHAPTER 2

Beam Propagation through Random Medium

This chapter explains the structure of the atmosphere and the related phenomena that affect the light beam when propagating. Also, presents the theoretical background of beam propagation in a random medium. Finally, gives a brief literature review of the studies

2.1 Atmosphere

The gaseous envelope that surrounds the Earth from all sides is the so-called atmosphere. Atmosphere consists of nitrogen, oxygen, water vapour, carbon dioxide, methane, nitrous oxide, and ozone. Depending on the temperature variation and the density, the atmosphere is divided into five layers, namely troposphere, stratosphere, mesosphere, ionosphere, and exosphere as shown in Figure 2.1 [7].

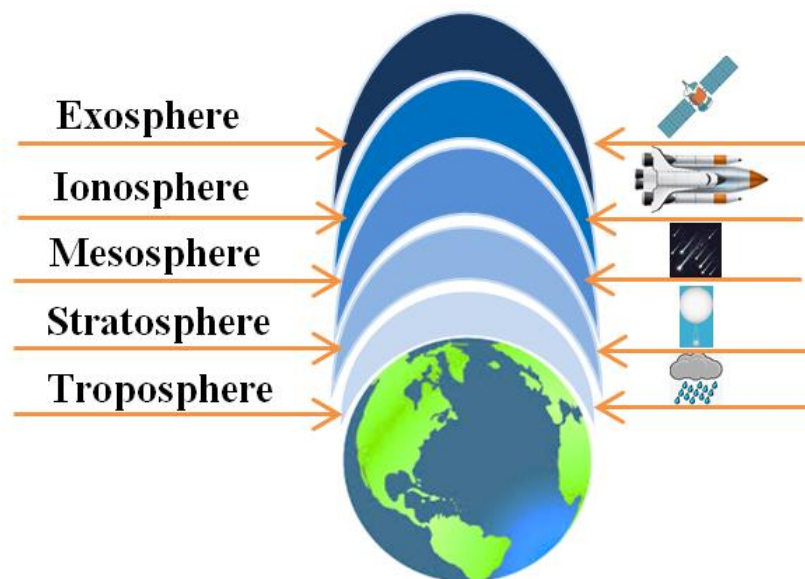


Figure 2.1 Atmospheric Layers

2.2 Atmospheric Turbulence

In atmosphere, the observed temperature and wind velocity changes give rise to a change the atmosphere refractive index which is known as *atmospheric turbulence*. These changes effect the optical beam travels in the atmosphere by causing a temporal irradiance fluctuations (scintillation) and phase fluctuations [7]. Figure 2.2 presents a schematic of Propagation of optical beams in atmospheric turbulence.

In optical links, the effect of atmospheric turbulence was studied using a statistical approach. The statistical approach assumes that within certain scale sizes the point separations have to be *statistically isotropic* and to have a *statistical homogeneity*. When the point to point correlations are controlled only by the magnitude of the vector separation between the observation points then the random fluctuations are statistically isotropic. Furthermore, if the random fluctuations have a constant mean and their correlations are independent of the observation point then they are statistically homogeneous [7, 24].

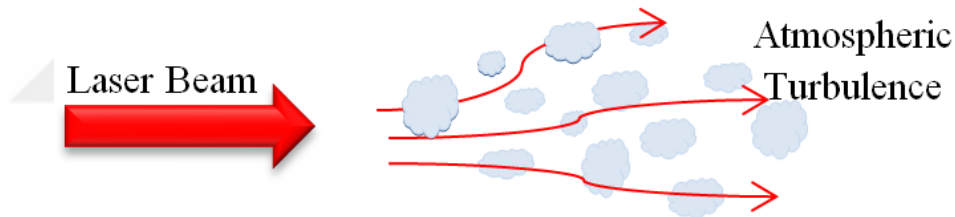


Figure 2.2 Propagation of optical beams in atmospheric turbulence

Atmospheric turbulence is a non-linear process that is governed by Navier-Stokes equations. Due to the difficulties of solving these equations, a statistical theory of turbulence was developed by Kolmogorov in 1941 [25, 26] Considering the *energy cascade theory* of turbulence shown in Figure 2.3, where L_0 refers to the outer scale of turbulence and l_0 refers to the turbulence inner scale and the eddies in between form the sub-range. If the scale sizes are smaller than l_0 then the turbulent eddies disappear and the remaining energy dissipates as heat. The scale sizes smaller than L_0 are assumed to be statistically homogenous and isotropic [7].

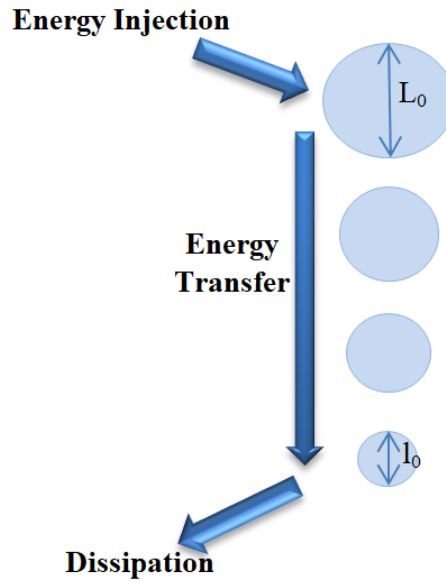


Figure 2.3 The Kolmogorov cascade theory of turbulence

2.3 Weak and Strong Turbulence Conditions

The classification of the theoretical theories that study the propagation of light in turbulent atmosphere is based on the strength of turbulence. Rytov variance is the parameter that distinguishes whether the turbulence level is weak or strong.

$$\sigma_R^2 = 1.23 C_n^2 k^{7/6} L^{11/6} \quad (2.1)$$

where C_n^2 represents the refractive index structure constant, k is the wave number ($k = 2\pi/\lambda$), λ is the operating wavelength and L refers to the propagation distance.

The value of Rytov variance either $\sigma_R^2 < 1$, $\sigma_R^2 \approx 1$ or $\sigma_R^2 \gg 1$ these values refer to weak turbulence, moderate turbulence and strong turbulence respectively [7, 27].

2.4 Power Spectrum Models for Optical Turbulence

A three dimensional Fourier transform relates the spatial power spectrum density to the covariance function due to the assumption of the statistical approach as:

$$\Phi_n(k) = \frac{1}{(2\pi)^3} \iiint_{-\infty}^{\infty} B_n(R) \exp(-i\mathbf{K} \cdot \mathbf{R}) d^3R = \frac{1}{2\pi^2 k} \int_0^{\infty} B_n(R) \sin(\kappa R) R dR \quad (2.2)$$

where R is the distance separating between two points, $\kappa = |\mathbf{K}|$ is the scalar wave number.

$$; B_n(R) = \frac{4\pi}{R} \int_0^{\infty} \kappa \Phi_n(\kappa) \sin(\kappa R) d\kappa \quad (2.3)$$

One of the widely adopted models of the power spectral density is the *Kolmogorov power-law spectrum* that is expressed as [7]

$$\Phi_n(k) = 0.033 C_n^2 \kappa^{-11/3} \quad 1/L_0 \ll \kappa \ll 1/l_0 \quad (2.4)$$

In the theoretical calculations Kolmogorov spectrum is widely used as a result of its simple formula. Although some calculations assume that the outer scale is infinity and the inner scale is small, while Kolmogorov spectrum has specific limits as shown in equation (2.3). Accordingly, *Tatarskii spectrum*, which includes the range of $\kappa > 1/l_0$, is introduced and given as [7]

$$\Phi_n(k) = 0.033 C_n^2 \kappa^{-11/3} \exp\left(-\frac{\kappa^2}{\kappa_m^2}\right) \quad \kappa \gg 1/L_0 \quad (2.5)$$

where $\kappa_m = 5.92/l_0$. If the limit $1/L_0 \rightarrow 0$ ($L_0 \rightarrow \infty$) then this spectrum has a singularity at $\kappa = 0$.

In practice, the modifications of Kolmogorov spectrum and Tatarskii spectrum are introduced to make them finite and isotropic for wave numbers $\kappa < 1/L_0$. If the modifications were applied by modeling the turbulence as statistically homogeneous and isotropic over all the wave numbers, then the power spectral density is modelled using von-Karman spectrum that is defined as [7]

$$\Phi_n(\kappa) = 0.033C_n^2\kappa^{-11/3} \frac{\exp(-\kappa^2/\kappa_m^2)}{(\kappa^2 + \kappa_0^2)^{11/6}} \quad 0 \leq \kappa < \infty \quad (2.6)$$

where $\kappa_0 = C_0/L_0$, C_0 refers to a scaling constant with a value chosen according to the application.

2.5 Propagation of Vortex Beams in a Turbulent Atmosphere

In FSO links, apart from all the attractive advantages, the environmental challenges that are caused by the propagation medium are inevitably encountered. Thus, studying the effect of these phenomena on the light beams is a critical issue for the FSO links. The Gaussian–Schell vortex and elliptical vortex beams are both able to improve the system performance due to their ability to reduce the scintillation levels [28, 29]. The system performance has been improved due to the reduction of the scintillation level of higher topological charge Laguerre-Gaussian vortex and combined Gaussian-vortex beams [30, 31]. Six different types of vortex beams has been investigated in strong turbulence, this study revealed that as the values of topological charge increases the scintillation level decreases [32]. Vortex beams have been investigated from the perspective of their propagation in turbulent atmosphere. Rytov approximation theory and the non-Kolmogorov turbulence model have been utilized to study the performance of Bessel Gaussian vortex beams propagating in a subway tunnel [33]. The analytic method has been used to evaluate the propagation factor and analyze the beam quality of the partially coherent flat-topped vortex beams propagating in atmospheric turbulence [34]. The average intensity of the flat-topped vortex hollow beam propagating in oceanic turbulence has been investigated using the formulation of extended Huygens-Fresnel diffraction integral [35]. The topological charge conservation and the propagation of the Laguerre vortex beam through atmospheric turbulence were studied in [36]. In [37] the propagation of partially coherent flat-topped vortex hollow beam in oceanic turbulence was examined using the extended Huygens–Fresnel diffraction integral. The extended Huygens-Fresnel diffraction integral was used to investigate the intensity of flat-topped vortex hollow beams in atmospheric turbulence in [38]; this study was limited to only the effect of the topological charge and the beam order on the intensity

profile at the low operating wavelength when the beam travel up to 3 km. On the other hand, the propagation of Bessel Gaussian vortex beam in atmospheric turbulence was using the extended Huygens-Fresnel principle, and only the effect of topological charge was explored [39]. The effect of the source parameters on the detection probability of partially coherent Bessel Gaussian vortex beams in anisotropic turbulence was studied [40]. The propagation of partially coherent Bessel–Gaussian beams in turbulent atmosphere was investigated via the extended Huygens–Fresnel principle [41]. To the best of our knowledge, the researches undertaken so far has been restricted to partially coherent flat-topped vortex hollow beam and partially coherent Bessel Gaussian vortex or studying specific parameters depending on complex techniques, hence no detailed research demonstrating the effectiveness of flat-topped Gaussian vortex beam and Bessel Gaussian vortex beam when propagating in turbulent atmosphere.

CHAPTER 3

Propagation of Vortex Beams in Atmosphere

This chapter covers the theoretical steps that are followed to model the atmospheric turbulence and to calculate the scintillation level of the vortex beams, also the design of the random phase screens model and its constraints. Finally, it represents the mathematical expressions of the studied vortex beams and their profiles with different parameters.

3.1 Introduction

The interest that vortex beams have acquired recently was due to the existence of orbital angular momentum (OAM), which is a novel method of communication applied in fiber and free-space optical communications [1, 2]. Vortex beams have an annular spatial profile with a dark spot at the centre (phase singularity); the dark spot size to the overall size is related to the topological charge value as the beam has a higher topological charge then it has a larger dark spot at its centre. These beams have a helical phase structure (spiral) along the propagation axis, due to this property vortex beams carry OAM of $m\hbar$.

These optical vortices can be expressed by $\exp(-im\theta)$, where the value of the topological charge “ m ” quantifies the phase front helicity and defines the direction of the wavefront along the propagation axis. These characteristics are in contrast with the conventional beams. The spatial profile, phase, and wavefront of the vortex beam are compared with that of Gaussian beam in Figure 3.1 [42, 43].

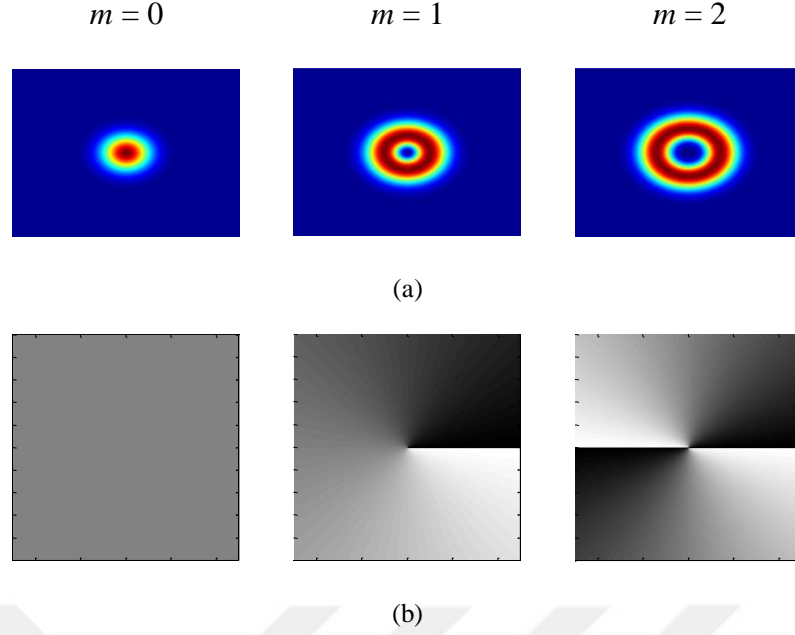


Figure 3.1 Vortex beam vs. Gaussian beam (a) spatial profile (b) phase

3.2 Turbulence Modeling

The use of wave-optics to model the propagation of light beams in a turbulent atmosphere is a combination Fourier transform and random phase screen model. The free-space propagation of the light beam can be efficiently simulated via Fourier transform [30]. Meanwhile, the phase fluctuations that caused by propagating in turbulence is modeled by dividing the total propagation distance into intervals of ΔL length separated by phase screen plans.

The received field of the vortex beam after propagating a distance L in a turbulence free medium (free space) is expressed by Huygens–Fresnel integral as [8]

$$u_{r_{fs}}(\mathbf{r}, L) = \frac{-jk}{2\pi L} \exp(jkL) \int_{-\infty}^{\infty} \int_{-\infty}^{\infty} u_s(\mathbf{s}) \exp\left[\frac{jk}{2L}(\mathbf{r} - \mathbf{s})^2\right] d^2\mathbf{s} \quad (3.1)$$

where $r = (r_x, r_y)$ is the receiver plane transverse coordinates, $s = (s_x, s_y)$ is the source plane transverse coordinates, L is the on-axis receiver plane location, and $k = 2\pi/\lambda$ refers to the wave number at the source wavelength λ .

Realizing that Eq. (2) has a two dimensional Fourier transform form, it can be written in as follows [44-47]

$$u_{r_{f_s}}(\mathbf{r}, L) = F^{-1}[F(u_s(s))F(h(r))] = F^{-1}[U_s(\mathbf{f})H(\mathbf{f})] \quad (3.2)$$

where $h(r)$ is the transfer function and F is the Fourier transform operator, F^{-1} is the inverse transform, $\mathbf{f} = (f_x, f_y)$ represents to the spatial frequency and $H(\mathbf{f})$ refers to the free space propagation transfer function with the following expression

$$H(\mathbf{f}) = \exp\left[jL\left(k - \frac{2\pi^2}{k}|\mathbf{f}|^2\right)\right] \quad (3.3)$$

The random phase screen model that we use includes the effect of atmospheric turbulence by dividing the propagation distance (L) up into N_s intervals ($\Delta L = L/N_s$) separated by thin phase screen planes. Accordingly, the field at the receiver plane on the m^{th} plane can be written as follows [46, 47]

$$u_r(\mathbf{r}, mL) = F^{-1}[F[u_s(\mathbf{r}, (m-1)\Delta L)\exp(j\phi(\mathbf{r}))]H(\mathbf{f})] \quad (3.4)$$

where $\phi(\mathbf{r})$ states the phase power spectral density of the individual screens of random phase distribution, in this study the Von-Karman spectrum is utilized with a power spectral density of [48]

$$\Phi_\phi(\mathbf{f}) = \frac{0.0036LC_n^2k^2L_0^{11/3}}{(L_0^2|\mathbf{f}|^2 + 1)^{11/6}} \exp[-1.1265l_0^2|\mathbf{f}|^2] \quad (3.5)$$

where C_n^2 denotes the refractive index structure constant, L_0, l_0 are the outer and inner scales of turbulence respectively.

Accordingly, the averaged intensity of the beam at the receiver plan can be found by multiplying the receiver field with its complex conjugate and expressed as follows

$$\langle I_r(\mathbf{r}, L) \rangle = \frac{1}{N_r} \sum_{i=1}^{N_r} u_r(\mathbf{r}, L)u_r^*(\mathbf{r}, L) \quad (3.6)$$

where where $\langle \rangle$ stands for the average, and $I_r(\mathbf{r}, L)$ is the intensity of the received field. Theoretically the averaging limit “ N_r ” approaches infinity, however, practically it is a turbulence dependent term and keeping it around 500 is sufficient [48-50].

3.3 Scintillation Expressions

The propagation medium in optical communications links is atmosphere, thus the refractive index fluctuations (turbulence) is one of the well-known phenomena. Accordingly, when light beams propagate in atmosphere, they face intensity fluctuations (scintillation). These fluctuations substantially degrade the probability of error performance of the system.

The scintillation index of a receiver plane located at L km can be expressed as [48]

$$b^2(\mathbf{r}, L) = \frac{\langle I_r^2(\mathbf{r}, L) \rangle}{\langle I_r(\mathbf{r}, L) \rangle^2} - 1 \quad (3.7)$$

Equation (3.7) can be solved either via Rytov approximation or extended Huygens Fresnel principle; however, both ways necessitate lengthy derivations.

The scintillation index in equation (3.7) is known as point-like scintillation which will turn into aperture averaged scintillation (power scintillation), if the side length, L_a of the square receiver capture area is less than $(0.5\lambda L)^{0.5}$ [45, 47]. This aperture averaged scintillation is expressed as follows

$$b^2(L) = \frac{\langle P_r^2(L) \rangle}{\langle P_r(L) \rangle^2} - 1 ; P_r(L) = \int_{-0.5L_a}^{0.5L_a} \int_{-0.5L_a}^{0.5L_a} I_r(r_x, r_y, L) dr_x dr_y \quad (3.8)$$

where $P_r(L)$ represents the received beam instantaneous power over a squared aperture which side length is L_a .

Consequently, determining the aperture averaged scintillation in terms of the aperture averaging and covariance is relatively difficult utilizing the analytical formulations. The mitigation of this difficulty is introduced by the use of random phase screen model by applying the summations and divisions. Moreover, the use of random phase screen model give chance to deal with almost all the beams and to extend the calculations of the single receiver point scintillation to aperture averaged scintillation.

3.4 Constructing the Random Phase Screen Model

The random phase screen approach alleviates all the difficult and lengthy formulations that analytical approaches own. This approach models the turbulent atmosphere by dividing the distance between the transmitter and the receiver into a shorter interval separated with a sufficient number of thin phase screens as illustrated in Figure 3.2. The distance between these screens is a critical element for designing the random phase screen model, thus it should be kept short enough to keep Rytov variance (equation (2.1)) of the accumulated turbulence in the range of weak turbulence. The other important elements in this design is the grid spacing, which should be kept greater than $\sqrt{\lambda L / N_s N_g}$ where N_s is the number of inserted phase screens and N_g is the number grid points that plays a critical role in the design and should be kept sufficiently high [51- 53].

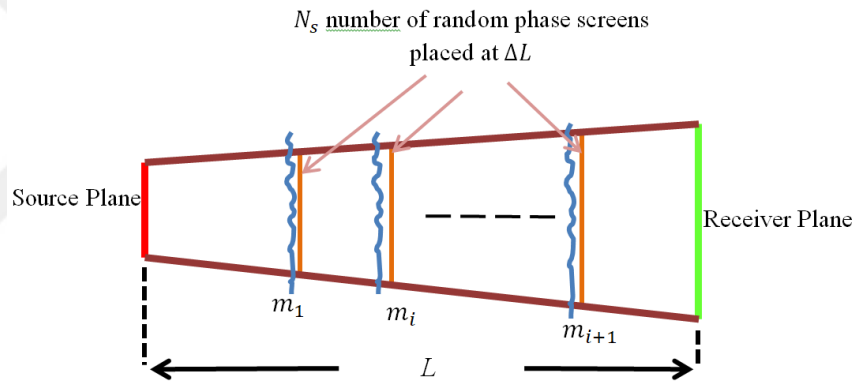


Figure 3.2 Random phase screen model

According to the equation (2.1) the turbulence strength of the studied cases is defined in Table 3.1 by calculating the Rytov variance.

Table 3.1 The turbulence strength of the studied cases

Set of Parameters (C_n^2, λ, L)		Rytov variance “ σ_R^2 ”	Turbulence Level
$10^{-14}, 1550 \text{ nm}$	0.5 km	0.0559	Weak Turbulence
	1 km	0.1991	
	3 km	1.4921	Strong Turbulence
	5 km	3.8063	
$10^{-14}, 830 \text{ nm}$	0.5 km	0.1158	Weak Turbulence
	1 km	0.4126	
	3 km	3.0920	Strong Turbulence
	5 km	7.8880	

Set of Parameters (C_n^2, λ, L)		Rytov variance “ σ_R^2 ”	Turbulence Level
$10^{-14}, 780 \text{ nm}$	0.5 km	0.1245	Weak Turbulence
	1 km	0.4436	
	3 km	3.3245	Strong Turbulence
	5 km	8.4810	
$10^{-14}, 632.8 \text{ nm}$	0.5 km	0.1589	Weak Turbulence
	1 km	0.5662	
	3 km	4.2432	Strong Turbulence
	5 km	10.8247	

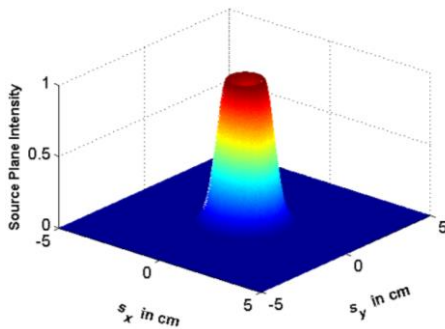
3.5 Vortex Beams under Consideration

Flat-topped beams (FT) can be obtained from the fundamental Gaussian beams by adding a parameter of flatness order. These beams spreading less when propagating this attractive feature made them important for some applications [54-56]. Accordingly, if these FT beams got the advantage of OAM will make these beams more attractive for a wide range of applications.

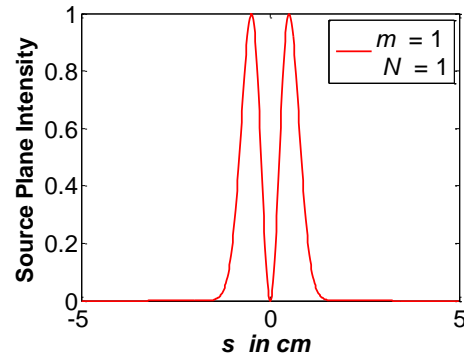
In this thesis the considered flat-topped Gaussian vortex beam in the source plane is expressed in the Cartesian coordinates system as [37]

$$u_s(s_x, s_y) = \frac{1}{N} \left(\frac{s_x + js_y}{\alpha_s} \right)^m \sum_{n=1}^N (-1)^{n-1} \binom{N}{n} \exp\left(-n \frac{s_x^2 + s_y^2}{\alpha_s^2}\right) \quad (3.9)$$

where m represents the topological charge, α_s is the source size and N is the beam order. Figure 3.3 represents the beam with different topological charges.



(a)



(b)

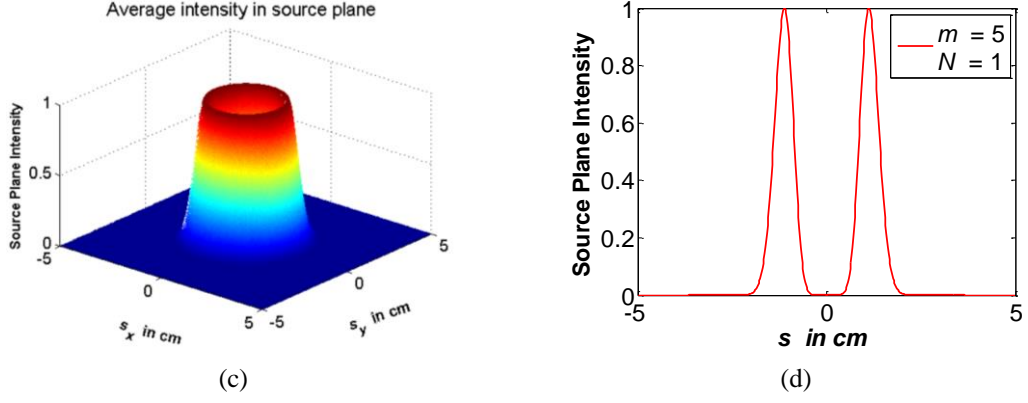


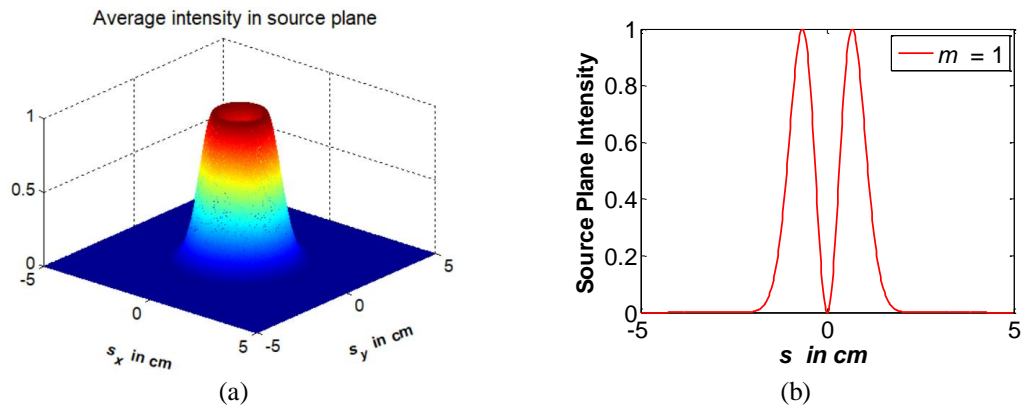
Figure 3.3 Flat-topped Gaussian vortex beam in the source plane (a, b) $m = 1, N = 1$, (c, d) $m = 5, N = 1$

Bessel Gaussian Vortex beam is an essential beam of the non-diffraction vortex beams, which can be generated easily with spatial light modulator [57]. Bessel Gaussian Vortex beams are very attractive for a wide range of applications like micromanipulation and quantum optical communications due to their non-diffracting property and self-healing characteristics [58].

The investigated Bessel Gaussian vortex beam in the source plane considered in the radial coordinates system as follows [40]

$$u_s(s, \phi) = \exp\left(-\frac{s^2}{\alpha_s^2}\right) J_m\left(\frac{s}{\alpha_s}\right) \exp(jm\phi) \quad (3.10)$$

where ϕ refers to the azimuthal angle. The Bessel Gaussian vortex beam in the source plane is plotted with different topological charges in Figure 3.4.



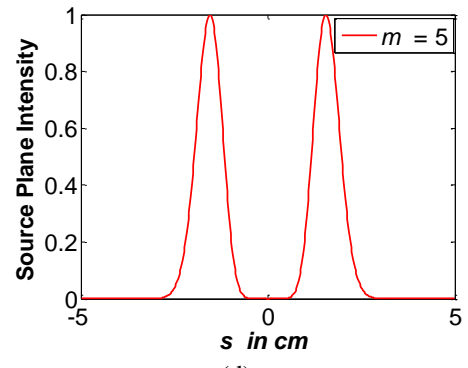
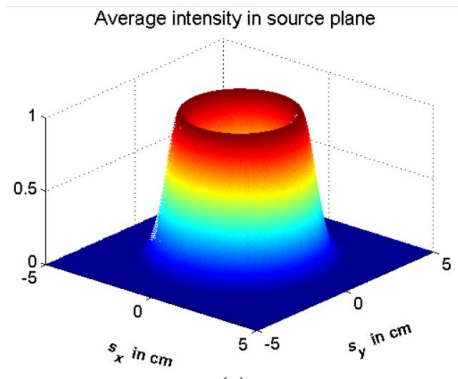


Figure 3.4 Bessel Gaussian vortex beam in the source plane (a, b) $m = 1$, (c, d) $m = 5$



CHAPTER 4

Effect of Beam Parameters on Vortex Beams Propagating in Atmospheric Turbulence

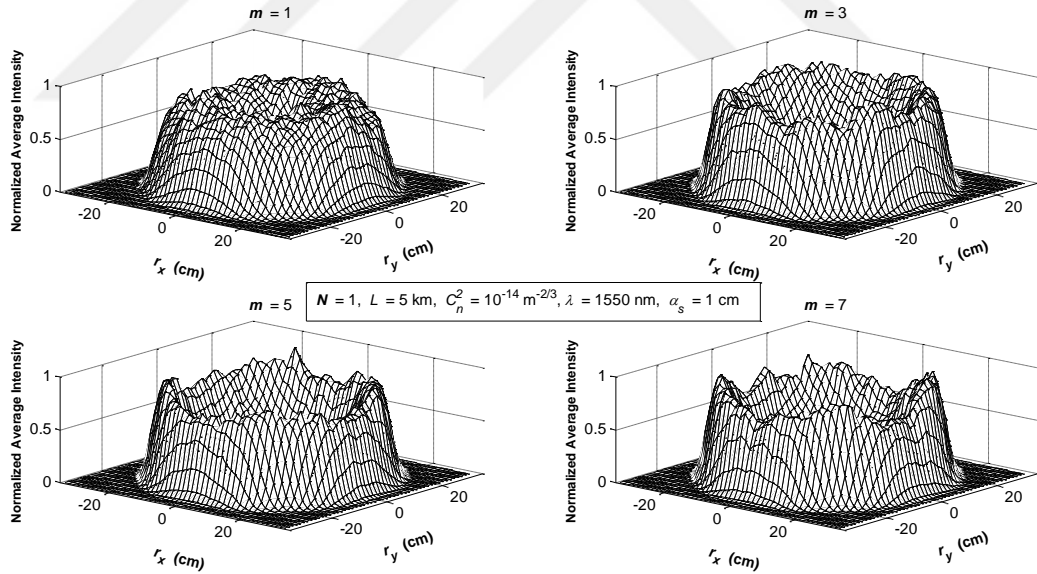
This chapter represents the design of the random phase screens model that is to be used to investigate the effect of beam parameters on the intensity profile of vortex beams propagating in atmospheric turbulence.

4.1 Random Phase Screens Design

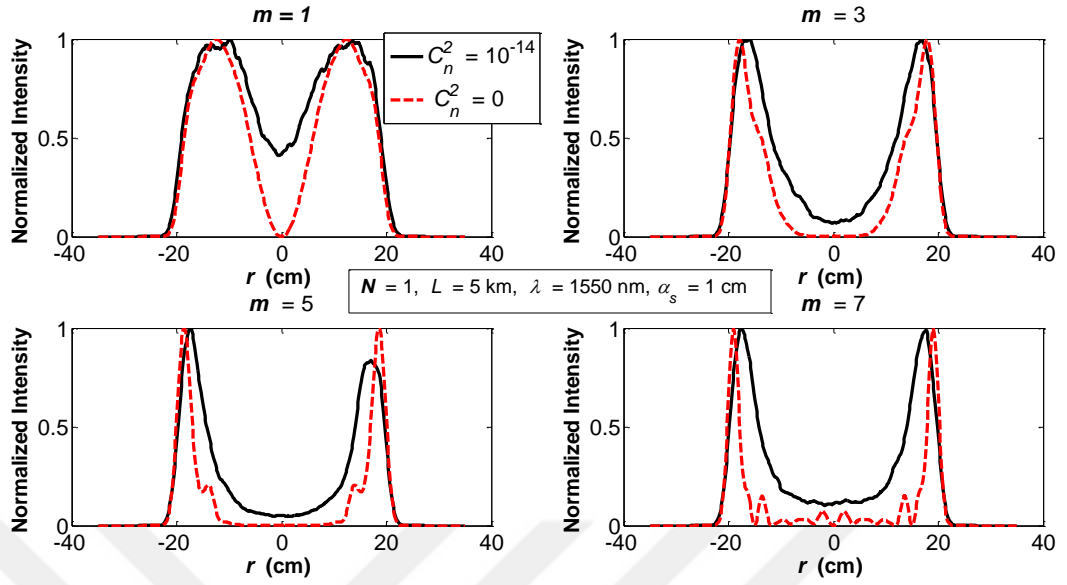
To obtain reliable results the propagation distance (L) divided into 30 intermediate phase screens with 512×512 grid size. The average intensity is presented in a cross line plots, where the averaging was taken over 500 simulation runs. The constant of refraction index structure of the atmospheric medium is considered as $10^{-14} m^{-2/3}$. The examined beam travels 5 km. The operating wavelength was chosen as 1550 nm since it is widely used in optical communication systems. The random phase screen setting is examined to cope with the constraints stated in [51, 52] sufficiently. The inner scale and the outer scale of the Von-Karman spectrum set to zero, and infinity respectively. A $10 \text{ cm} \times 10 \text{ cm}$ source plane is used to accommodate all the beam power efficiently. The effects of topological charge, beam order, propagation distance, source size and operating wavelength on the flat-topped Gaussian vortex beam propagating in a turbulent atmosphere are assessed and discussed. The evolution properties of the beam by comparing the intensity of the received beam propagated in turbulence with the same beam propagated in free space are evaluated.

4.2 Flat-topped Gaussian Vortex Beam

The effect of the topological charge (m) on the intensity profile of flat-topped Gaussian vortex beam with beam order ($N = 1$), source size ($\alpha_s = 1$ cm) and operating wavelength ($\lambda = 1550$ nm) after propagating 5 km in moderate turbulence ($C_n^2 = 10^{-14} \text{ m}^{-2/3}$) is illustrated in Figure 4.1. By comparing the intensity profile of the beam propagating in turbulence with the profile of the same beam propagating in free space, we can observe that beams with higher topological charges keep their initial profile better than the beams with lower topological charges. This result is in agreement with the analytical results in [37, 38], which proves that the designed random phase screen model works properly. As the topological charge increases some repels start to appear in the intensity profile of the beam propagating in the free space that is due to the averaging, by increasing the number of runs these repels will disappear. This result gives flat-topped Gaussian vortex beam an advantage over the other beams that eventually evolve to Gaussian profile [59].



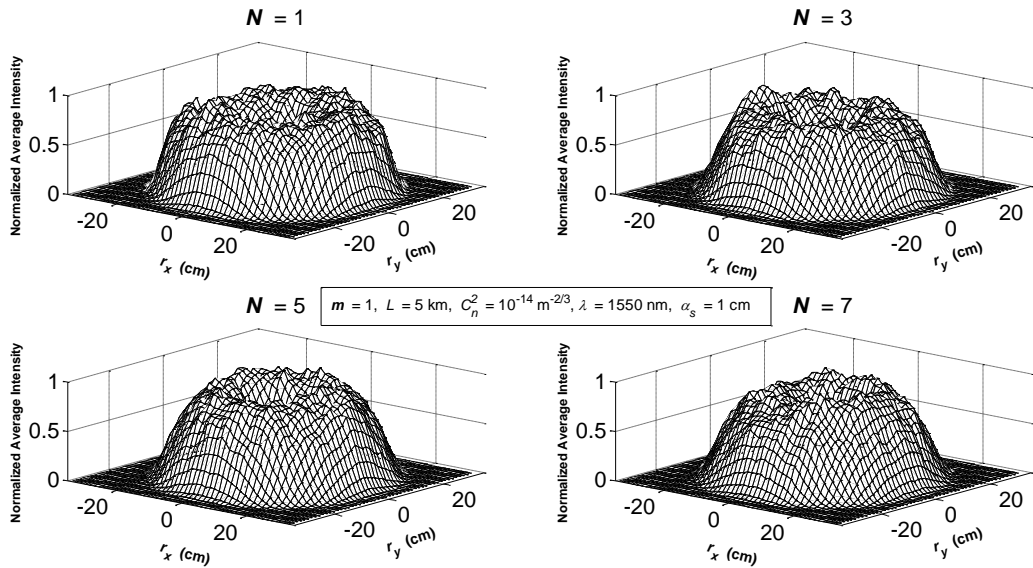
(a)



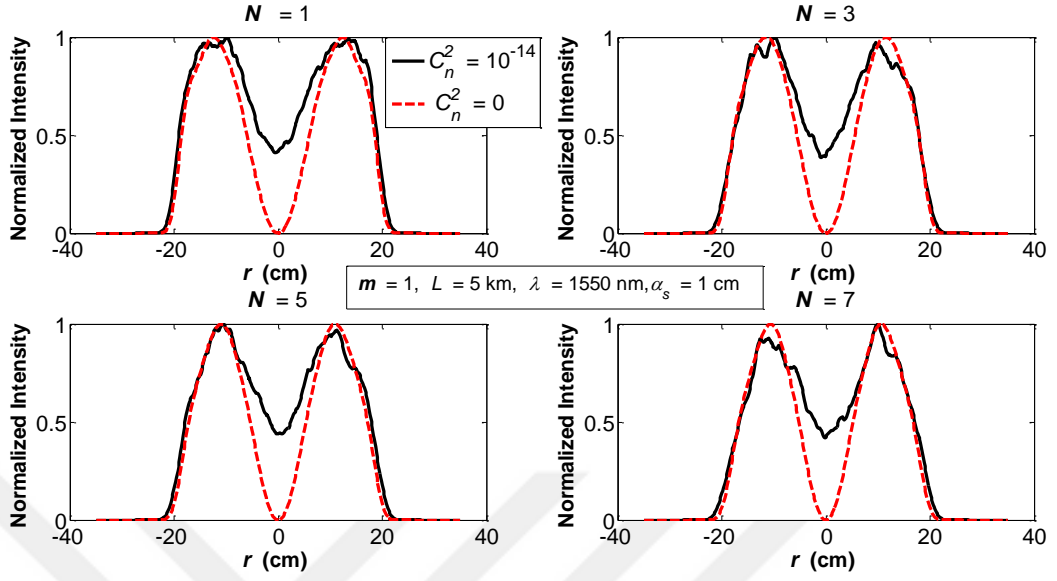
(b)

Figure 4.1 Received normalized average intensity of flat-topped Gaussian vortex beam propagating in turbulence at different topological charges (m)

The behavior of flat-topped Gaussian vortex beam with different beam orders is studied in Figure 4.2. The beam with topological charge $m = 1$ and 1 cm source size; propagates in moderate turbulence for 5 km is compared with the one propagates in free space. We noticed that the change in the beam order (N) does not have a significant effect on the intensity profile evaluation of the beam.



(a)



(b)

Figure 4.2 Received normalized average intensity of flat-topped Gaussian vortex beam propagating in turbulence at different beam orders (N)

The intensity profiles of flat-topped Gaussian vortex beam against different propagation distances are shown in Figure 4.3. In which as expected we can see that as the propagation distance increases the beam evolves to lose its hollow center. This is a reasonable result due to the fact that in turbulent medium the coherence length of the beam, given in [59], decreases in the form of $L^{-3/5}$ as the propagation distance increases [59, 60].

Figure 4.4 shows the variation of flat-topped Gaussian vortex beam profile against the source size (α_s) when the beam with topological charge ($m = 1$) and beam order ($N = 1$) propagates 5 km in moderate turbulence at operating wavelength of 1550 nm. As observed from the figure beams with bigger source sizes will evolve into Gaussian-like profiles faster than the ones with small source sizes.

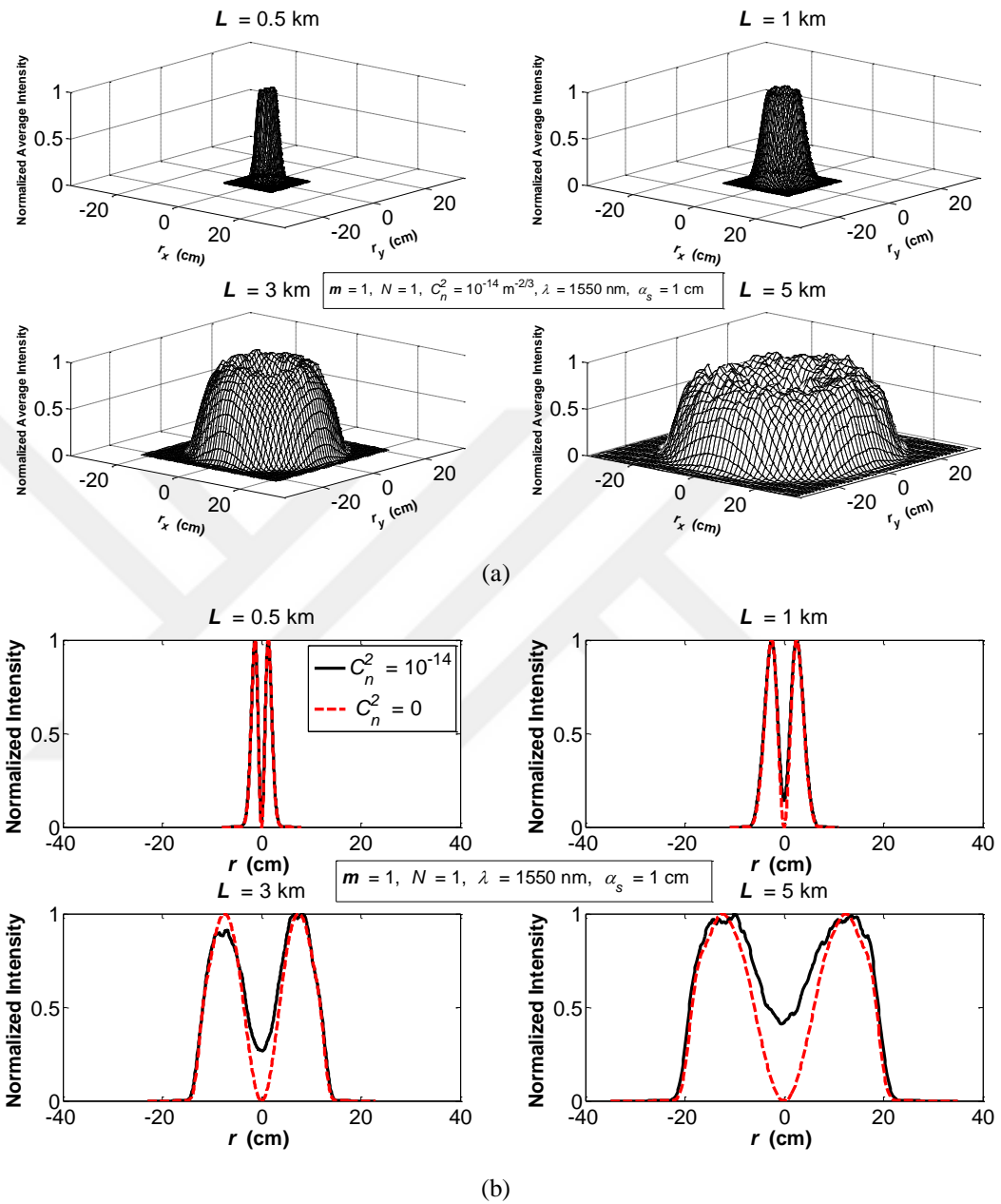
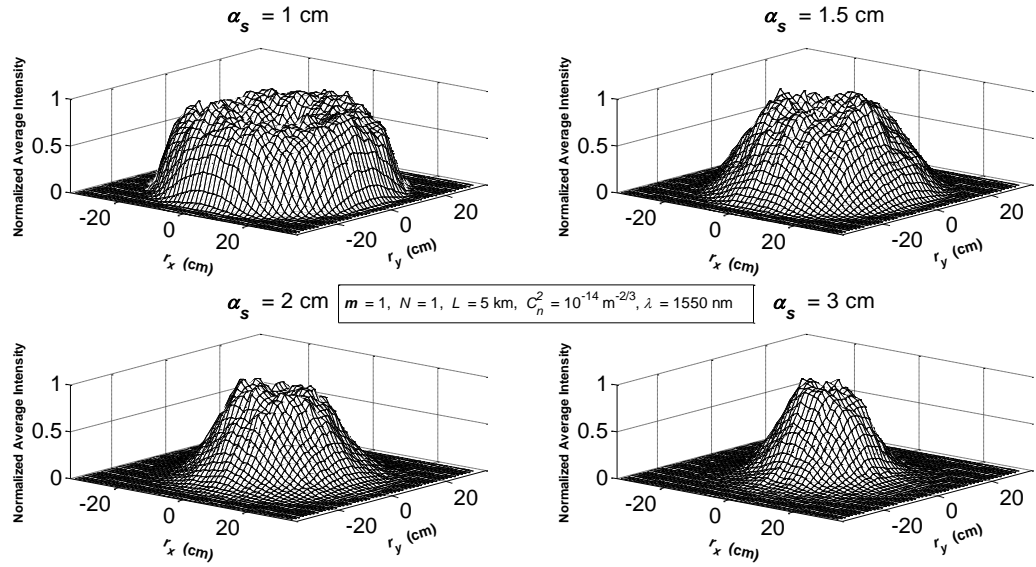
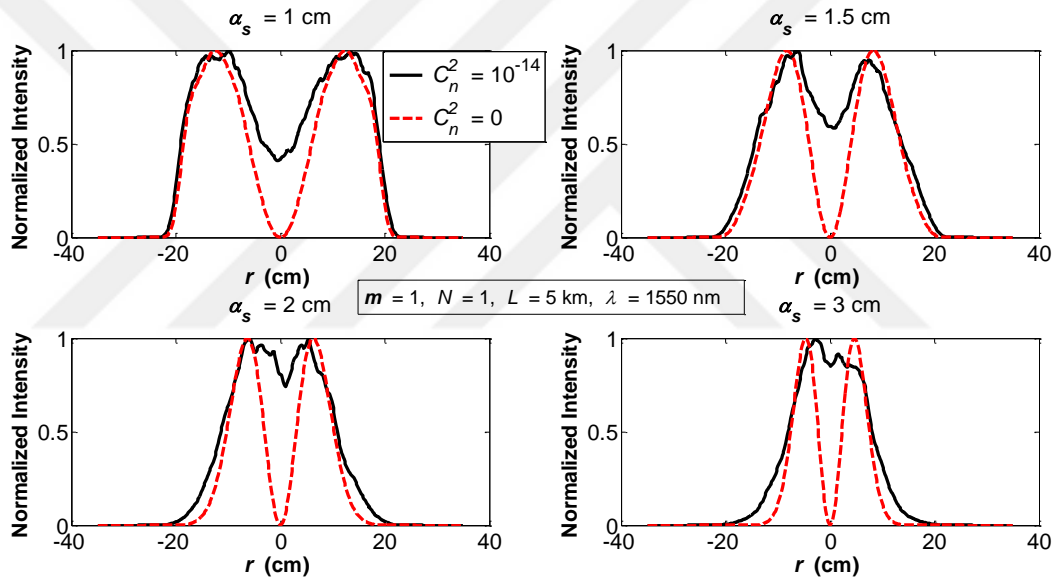


Figure 4.3 Received normalized average intensity of flat-topped Gaussian vortex beam propagating in turbulence at different propagation distances (L)



(a)



(b)

Figure 4.4 Received normalized average intensity of flat-topped Gaussian vortex beam propagating in turbulence at different source sizes (α_s)

The operating wavelength is an essential parameter in the communication links, for this reason four different wavelengths that are in used in the optical communication systems set to be investigated how they affect the flat-topped Gaussian vortex beam propagating in turbulent atmosphere. From Figure 4.5 we obtained that operating at higher wavelengths helps the beam keeping its original beam profile at moderate turbulence. According to [59, 60] operating at higher wavelengths increases the coherence length that helps the beam resist the turbulence effect.

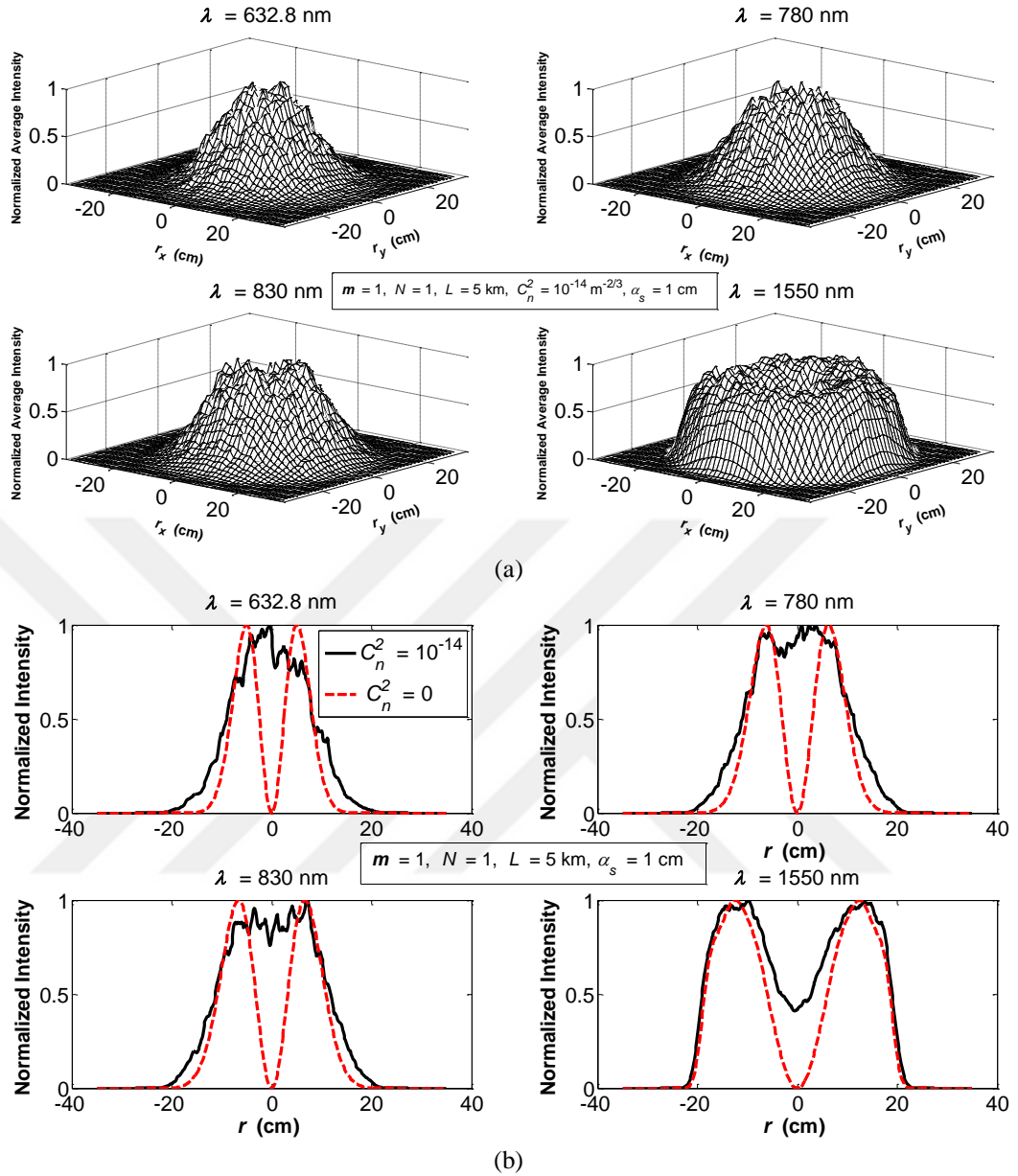
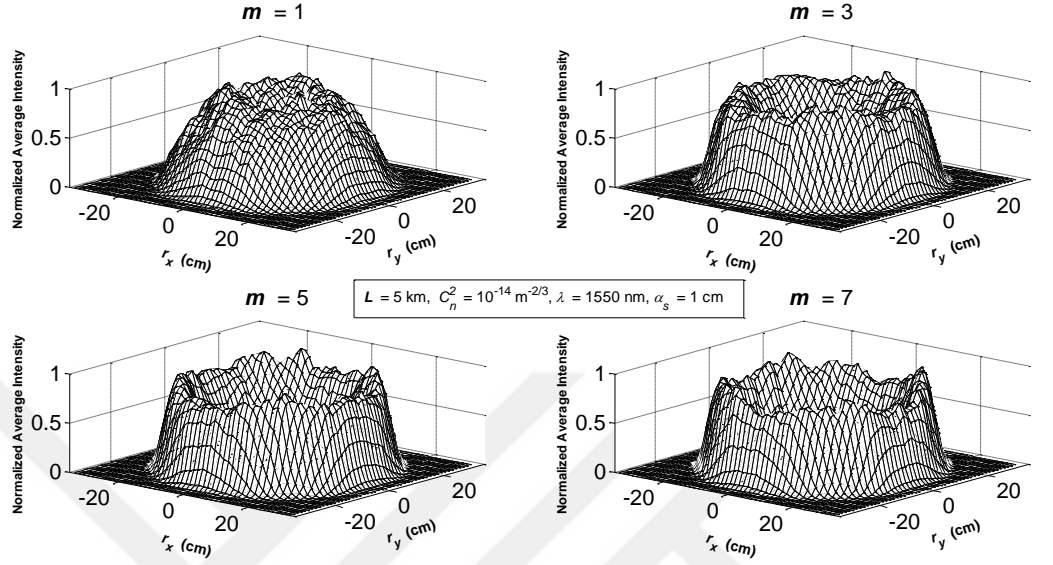


Figure 4.5 Received normalized average intensity of flat-topped Gaussian vortex beam propagating in turbulence at different operating wavelength (λ)

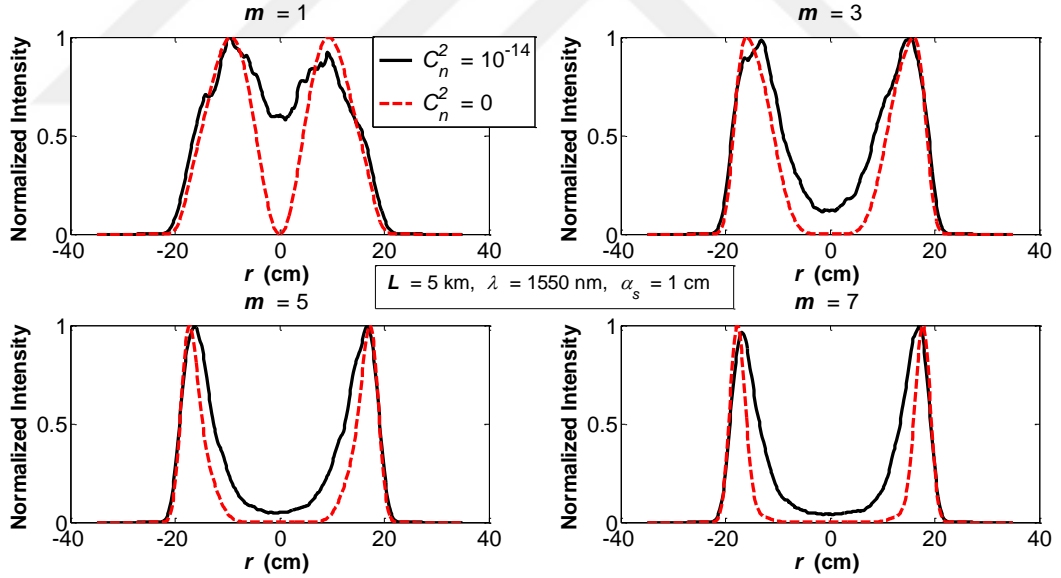
4.3 Bessel Gaussian Vortex Beam

The effect of the topological charge (m) on the intensity profile of Bessel Gaussian vortex beam with source size ($\alpha_s = 1$ cm) and operating wavelength ($\lambda = 1550$ nm) after propagating 5 km in moderate turbulence ($C_n^2 = 10^{-14} \text{ m}^{-2/3}$) is illustrated in Figure 4.6. By comparing the intensity profile of the beam propagating in turbulence with the profile of the same beam propagating in free space, we can observe that beams with higher topological charges keep their initial profile better than the beams

with lower topological charges. This result is in agreement with the analytical results in [37, 59], which proves that the designed random phase screen model works properly.



(a)



(b)

Figure 4.6 Received normalized average intensity of Bessel Gaussian vortex beam propagating in turbulence at different topological charges (m)

The intensity profiles of Bessel Gaussian vortex beam against different propagation distances are shown in Figure 4.7. In which as expected we can see that as the propagation distance increases the beam evolves to lose its hollow center. This is a

reasonable result due to the fact that in turbulent medium the coherence length of the beam, give in [59], decreases in the form of $L^{-3/5}$ as the propagation distance increases [59, 60].

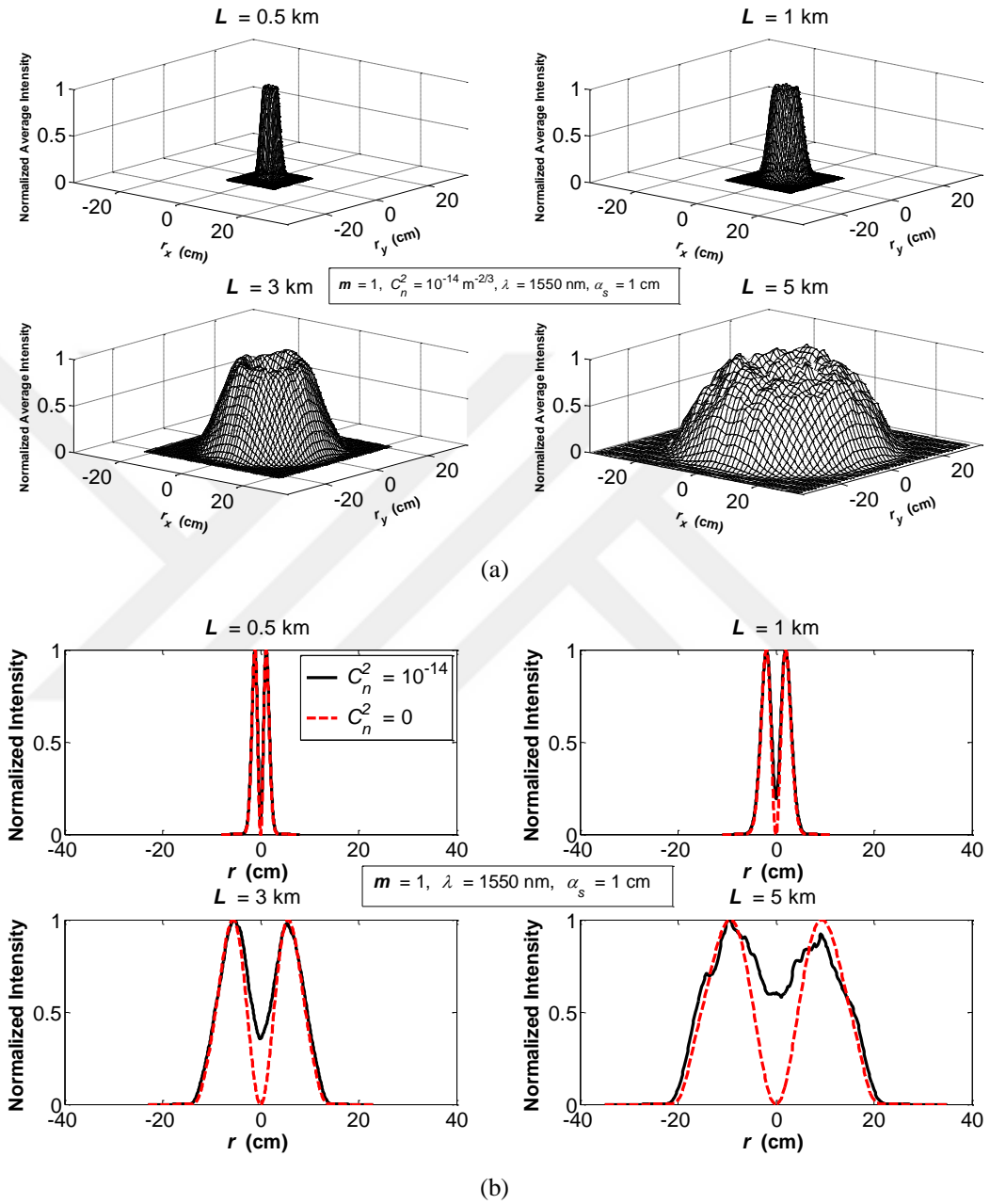


Figure 4.7 Received normalized average intensity of Bessel Gaussian vortex beam propagating in turbulence at different propagation distances (L)

Figure 4.8 shows the variation of Bessel Gaussian vortex beam profile against the source size (α_s) when the beam with topological charge ($m = 1$) and propagates 5 km in moderate turbulence at operating wavelength of 1550 nm. As observed from the

figure beams with bigger source sizes will evolve into Gaussian-like profiles faster than the ones with small source sizes.

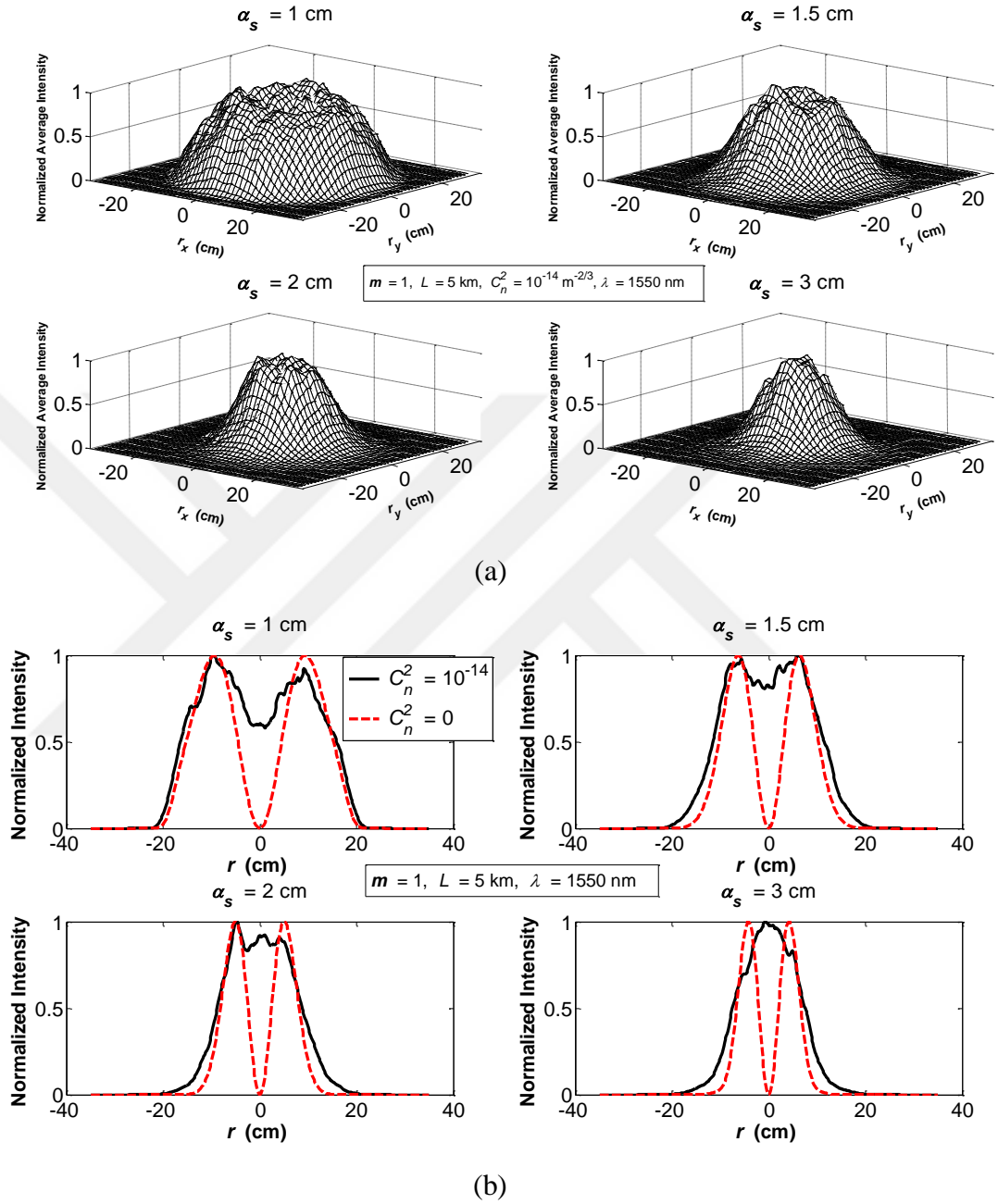


Figure 4.8 Received normalized average intensity of Bessel Gaussian vortex beam propagating in turbulence at different source sizes (α_s)

The operating wavelength is an essential parameter in the communication links, for this reason four different wavelengths that are in used in the optical communication systems set to be investigated how they affect the Bessel Gaussian vortex beam propagating in turbulent atmosphere. From Figure 4.9 we obtained that operating at

higher wavelengths helps the beam keeping its original beam profile at moderate turbulence. According to [59, 60] operating at higher wavelengths increases the coherence length that helps the beam resist the turbulence effect.

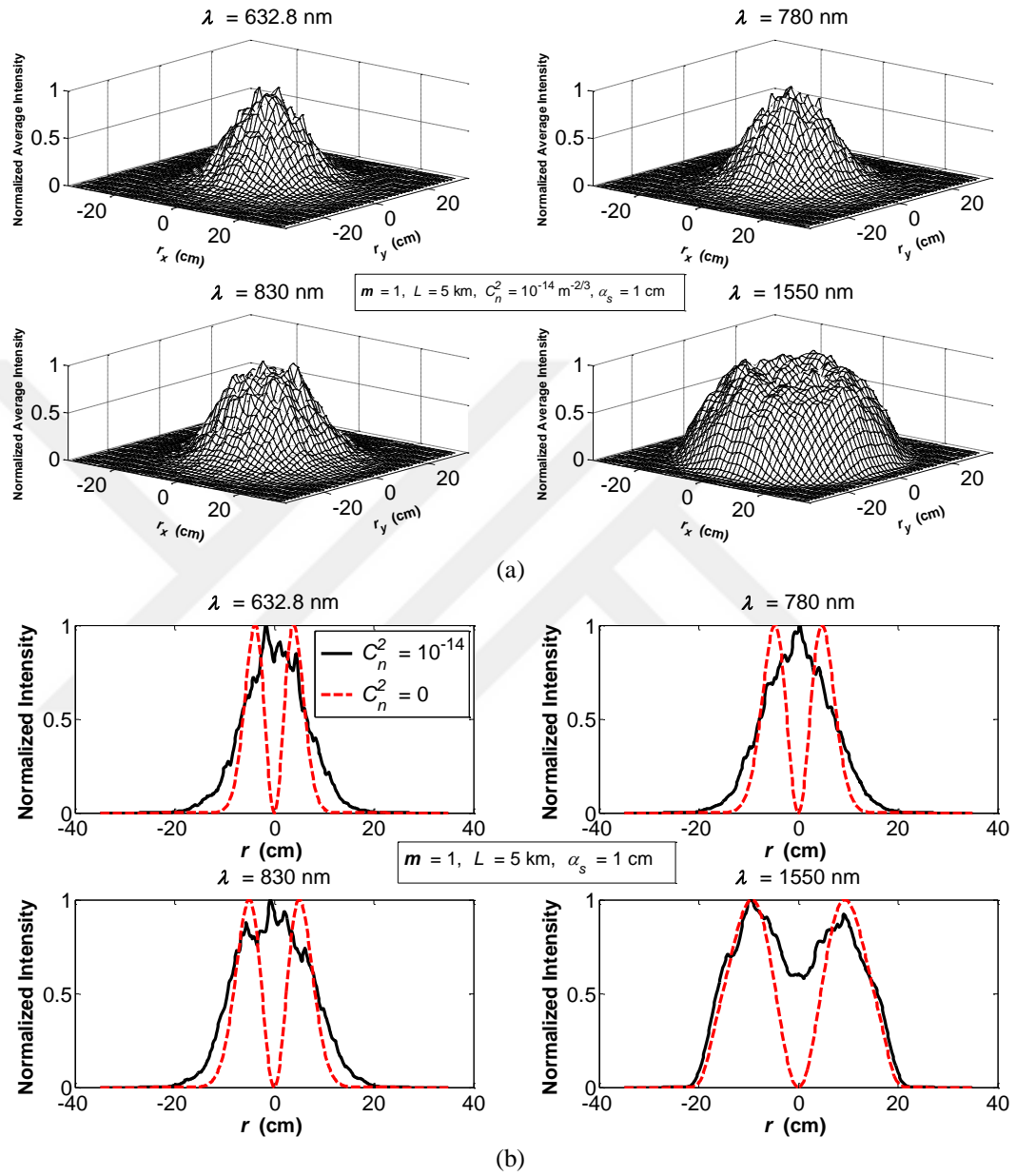


Figure 4.9 Received normalized average intensity of Bessel Gaussian vortex beam propagating in turbulence at different operating wavelength (λ)

CHAPTER 5

Effect of Beam Parameters on the Scintillation Properties of Vortex Beams

In this chapter, the design of the random phase screens model is introduced. Then, this model is to be used to examine the scintillation properties of the vortex beams under the consideration of different beam parameters.

5.1 Random Phase Screens Model

For the investigated results to be reliable, the propagation distance that ranges between 0.05 and 3.5 km, is divided into 20 intermediate phase plans with a 512×512 grid size, both on the source and receiver planes. The designed random phase screen model is tested to cope with the constraints given in the literature [51-53]. The results are presented in graphical plots obtained over 500 simulation runs which are considered to be adequate to reveal the theoretical limits of the curves [46, 61]. The inner scale and the outer scale of the Von-Karman spectrum are set to be zero and infinity, respectively. The atmosphere structure constant is considered as $10^{-14} \text{ m}^{-2/3}$. The source plane dimensions are set as $10 \text{ cm} \times 10 \text{ cm}$. The side length of the receiver square aperture (aperture size) is set to $N_a = 100$ grid points, which leads to a variable L_a . Figure 5.1 presents the receiver aperture side length variation versus the propagation distance, besides with the dividing line between the point-like and aperture averaged scintillation $(0.5\lambda L)^{0.5}$.

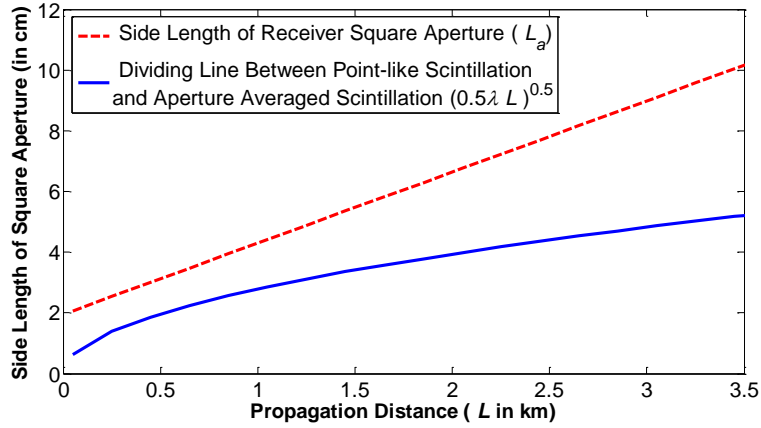


Figure 5.1 The receiver aperture side length variation versus the propagation distance

Figure 5.2 compares the scintillation properties of the flat-topped Gaussian vortex beam resulted from the designed random phase model with the one from the analytical formulation [61]. The comparison is at a fixed source size of $\alpha_s = 1$ cm, and an operating wavelength of 1550 nm, the aperture side length is that of Fig. 1 and the structure constant is $10^{-15} \text{ m}^{-2/3}$.

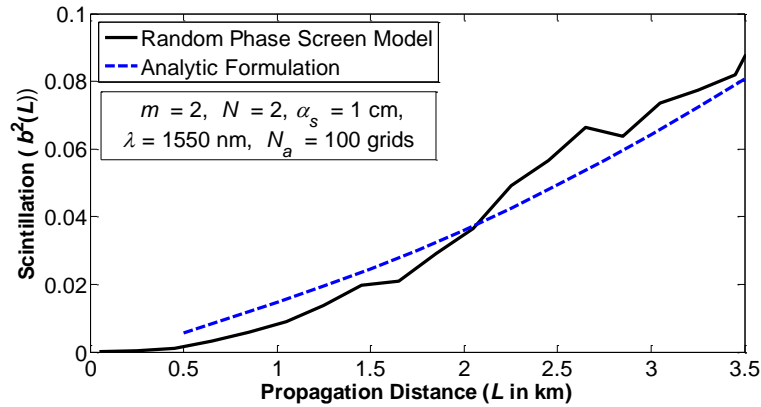


Figure 5.2 Comparing the scintillation of flat-topped Gaussian vortex beam from random phase screen model and analytic formulation

5.2 Scintillation Properties of Flat-topped Gaussian Vortex Beam

At a fixed, a beam order of $N = 2$, source size of $\alpha_s = 1$ cm, and operating wavelength of 1550 nm, the effect of the topological charge on the scintillation properties of flat-topped Gaussian vortex beam are examined as in Figure 5.3. Bearing in mind, the illustrated variation of the receiver aperture side length in Figure 5.1. Accordingly, as the propagation distance increases, flat-topped Gaussian vortex beams with higher topological charges start to have lower scintillation levels, which is slightly different from the usual expectation in which increasing the propagation distance rises the scintillation level. These findings are confirmed by the analytical derivatives of the propagation of flat-topped Gaussian vortex beams in the turbulent atmosphere [38, 60, 62], here the results showed that when the beams have higher topological charges they can preserve their intensity profile after propagating a distance in turbulence.

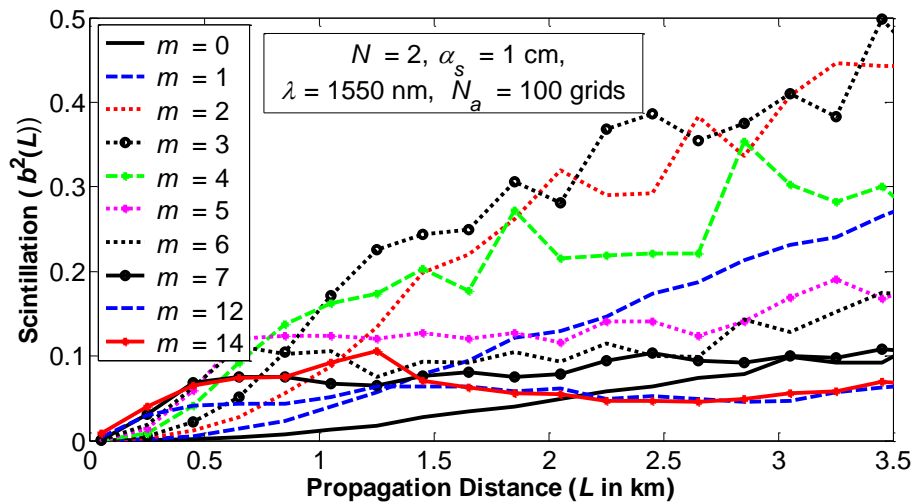


Figure 5.3 The effect of changing the topological charge on the scintillation properties of flat-topped Gaussian vortex beam

Observing Figure 5.4 reveals that the beam order of the flat-topped Gaussian vortex beam does not affect the scintillation levels of the beam, which has a topological charge of $m = 2$, source size of $\alpha_s = 1$ cm, and operating at a wavelength of 1550

nm. Thus, these findings confirm the results in [38], which observed that as the flat-topped Gaussian vortex beams with different beam orders propagate in a turbulent atmosphere their evolution properties are similar [62].

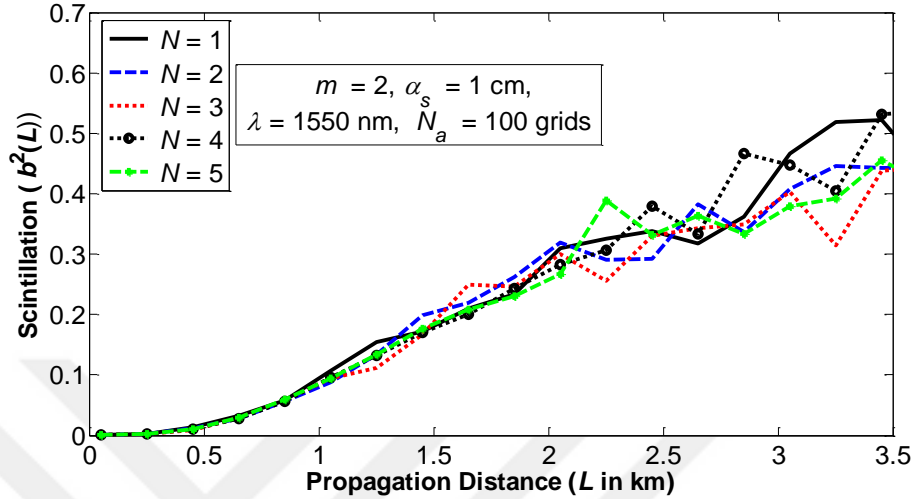


Figure 5.4 The effect of changing the beam order on the scintillation properties of flat-topped Gaussian vortex beam

Figure 5.5 shows that the scintillation of flat-topped Gaussian vortex beam decreases up to a certain level by increasing the source size then it saturates which somehow different from the situation of point-like scintillation. The examined beam has a topological charge $m = 2$, beam order $N = 2$, and operates at a wavelength of 1550 nm. These results are again govern by the variation of the aperture side length that given in Figure 5.1 [62]. It is assumed that an aperture is applied for source beams whose footprints exceed the 10 cm X 10 cm.

The effect of changing the length of the receiver aperture (in terms of grid points) on the scintillation properties the flat-topped Gaussian vortex beam is investigated in Figure 5.6. The result seems to be in line with the general expectation, that is, as the receiver aperture side length the scintillation level starts to decrease, since increasing the aperture side length allows the receiver to detect more wandering charge. The

beam that received with aperture opening of $N_a = 60$ is still on the region of aperture averaged scintillation according to the curve of $(0.5\lambda L)^{0.5}$ in Figure 5.1 [62].

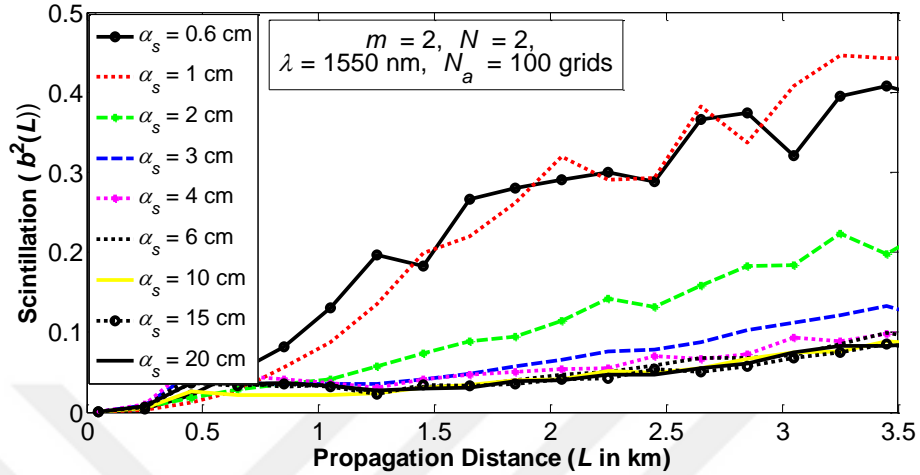


Figure 5.5 The effect of changing the source size on the scintillation properties of flat-topped Gaussian vortex beam

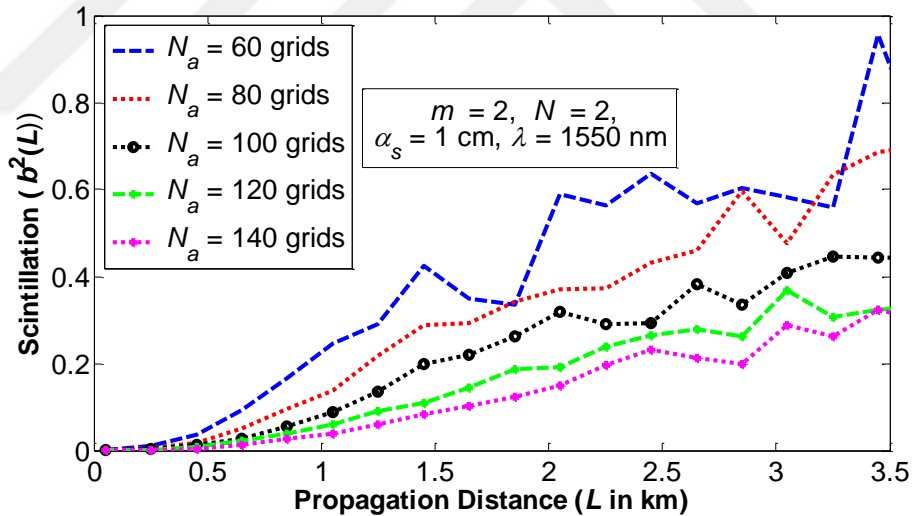


Figure 5.6 The effect of changing the side length of receiver aperture on the scintillation properties of flat-topped Gaussian vortex beam

Figure 5.7 displays that as the beam travels longer, the operating wavelength does not appreciably affect the scintillation level of the flat-topped Gaussian beam that has $m = 2$ as a topological charge, $N = 2$ as a beam order, and $\alpha_s = 1$ cm as a source size. These results are in agreement with the reported theoretical predictions

and measurements for the conditions of aperture averaged scintillation that is under investigation in this thesis [62, 63].

Figure 5.8 compares the scintillation properties of flat-topped Gaussian vortex beam the conventional Gaussian beam. Consequently, as both beams travel longer, flat-topped Gaussian vortex beams with higher topological charges have the advantage of decreasing the scintillation level, which is in agreement with the results in [32].

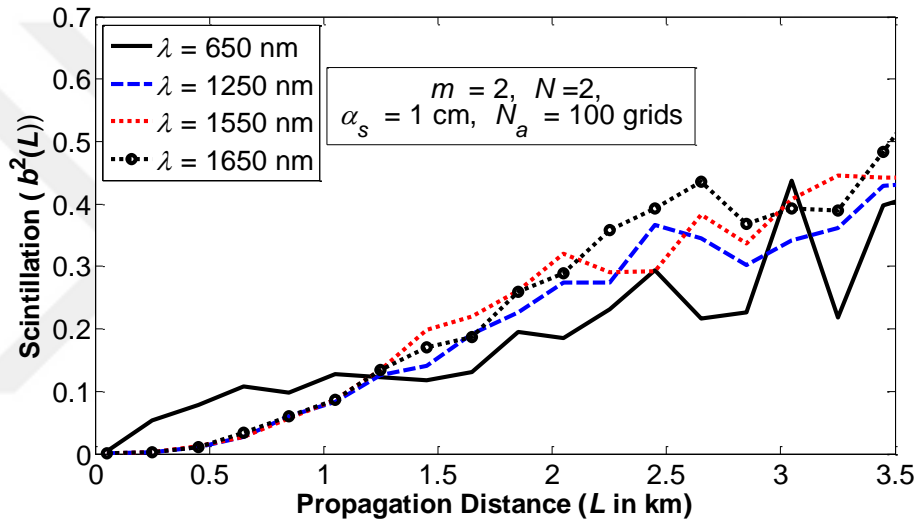


Figure 5.7 The effect of changing the operating wavelength on the scintillation properties of flat-topped Gaussian vortex beam

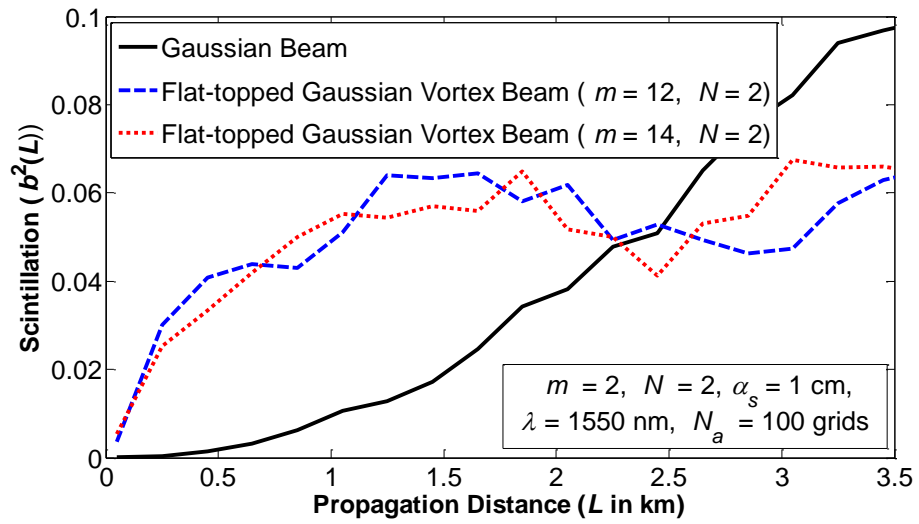


Figure 5.8 Comparing the scintillation properties of flat-topped Gaussian vortex beam with the Gaussian beam

CHAPTER 6

Conclusion and Suggestions

The random phase screen model is utilized to investigate the behaviour of flat-topped Gaussian vortex beam propagating in atmospheric turbulence. For the first time a detailed analysis of the beam parameters' effect on the intensity profile of flat-topped Gaussian vortex beam and Bessel vortex beam propagating in a turbulent atmosphere are investigated. Accordingly, it is observed that vortex beams with a higher topological charge will keep its original shape. The beam order changes do not affect the beam profile for the flat-topped Gaussian vortex beam. As the propagation distance increases the effect of turbulence will be stronger. Beams with bigger source sizes will evolve to the Gaussian-like beam. Operating at higher wavelengths will help the beam keeping its initial profile. The findings are in good agreement with the analytical expectations in literature. Accordingly, the obtained results will be very useful in the analysis and design of optical communication links in the future applications.

Moreover, the effect of beam parameters is examined on the aperture averaged scintillation properties of flat-topped Gaussian vortex beam propagating atmospheric turbulence. Utilizing a random phase screen method the atmospheric turbulence is modelled. Consequently, as the flat-topped Gaussian vortex beams travel longer distances, the higher the topological charges of the beam the lower the scintillation levels. Furthermore, the scintillation level of the flat-topped Gaussian vortex beam decreases when beams have bigger source sizes. Increasing the receiver aperture side length improves the scintillation properties of the beam. The beam order has no significant effect on the scintillation properties. As the beam travels longer, the operating wavelength does not appreciably affect the scintillation level of the flat-topped Gaussian beam. As the propagation distance increases, a flat-topped Gaussian vortex beam with high topological charges have the advantage over the conventional Gaussian beam.

Consequently, the effect of the beam parameters on the phase distributions of the vortex beams propagating in the turbulent atmosphere will be investigated in detail. Such a study will give an opportunity to understand the advantages of these beams to be used in the next generations of the FSO systems. In addition, the effect of amplitude and phase corrections on the FSO link that uses a vortex beam will be studied. For the future studies will be reserved on the propagation range of 5 km.



REFERENCES

- [1] **Hurdeman, A.A.** (2003), *The Worldwide History of Telecommunications*, John Wiley & Sons, Inc., Publication.
- [2] **Hutt, D.L., Snell, K.J., Belanger, P.A.** (1993), Alexander Graham Bell's Photophone, *Optics and Photonics News*, Vol. 4, Issue 6, pp. 20-25.
- [3] **Kaushal, H.** et. al. (2017), *Free Space Optical Communication*, Springer.
- [4] **Mansour, A.** et al. (2017), New challenges in wireless and free space optical communications, *Optics and Lasers in Engineering*, 89, 95–108.
- [5] **Chowdhury, M. Z.** et. al. (2018), A Comparative Survey of Optical Wireless Technologies: Architectures and Applications, *IEEE ACCESS*, 9819-9840.
- [6] **Alimi, I.** et. al. (2017), Challenges and Opportunities of Optical Wireless Communication Technologies, Chapter, <http://dx.doi.org/10.5772/intechopen.69113>.
- [7] **Kaushal, H.** et. al. (2017), Overview of Wireless Optical Communication Systems, DOI: 10.1007/978-81-322-3691-7_1,
- [8] **Andrew L.C. and Phillips R.L.,** (2005), *Laser Beam Propagation Through Random Media*, SPIE Press: Bellingham, WA.
- [9] **Wang, F.** et. al. (2015) Propagation of Partially Coherent Beam in Turbulent Atmosphere: A Review, *Progress In Electromagnetics Research*, Vol. 150, 123–143.
- [10] **Padgett, M.** et. al. (2004), Light's Orbital Angular Momentum, *American Institute of Physics, Physics Today*, 35-40.
- [11] **Poynting, J.** (1909), The Wave Motion Of A Revolving Shaft, And A Suggestion As To The Angular Momentum In A Beam Of Circularly Polarised Light, *Proc. R. Soc. Lond. A Ser. A* 82, 560–567.
- [12] **Beth, R.** (1936), Mechanical Detection and Measurement of the Angular Momentum of Light, *Phys. Rev.* 50, 115–125.

- [13] **Allen, L.** et. al. (1992), Orbital Angular-momentum of Light and the Transformation of Laguerre–Gaussian Laser Modes, *Phys. Rev. A* 45, 8185–8189.
- [14] **Willner, A.E.** et. al. (2015), Optical Communications Using Orbital Angular Momentum Beams, *Advances in Optics and Photonics* 7, 66–106.
- [15] **Yao, A.M. and Padgett, M.J.** (2011), Orbital angular momentum: origins, behaviour and applications, *Advances in Optics and Photonics* 3, 161–204.
- [16] **Liua, X.** et. al. (2019), Review on Vortex Beams with Low Spatial Coherence, *Advances in Physics: X*, VOL. 4, NO. 1, 1626766.
- [17] **Feng, L.** et. al. (2019), A Review of Tunable Orbital Angular Momentum Modes in Fiber: Principle and Generation, *Appl. Sci.*, 9, 2408; doi:10.3390/app9122408.
- [18] **Verbeeck, J.** et. al. (2010), Production and Application of Electron Vortex Beams, *Nature*, 467, 16, 301-304.
- [19] **Barnett, S.** et. al. (2017), Optical orbital angular momentum, *Phil. Trans. R. Soc. A* 375:20150444 (2017).
- [20] **Ashkin A.** (2001), *Optical trapping and manipulation of neutral particles using lasers*. Singapore: World Scientific.
- [21] **Shen, Y.** et. al. (2018), Recent Advances on Tunable Vortex Beam Devices for Biomedical Applications, *Biomedical Journal of Scientific & Technical Research*, 9, 3.
- [22] **Wang, J.** et. al (2019), Twisted optical communications using orbital angular momentum, *Sci. China-Phys. Mech. Astron.* 62, 3, 034201.
- [23] **Ren Y.** et al. (2015), Turbulence compensation of an orbital angular momentum and polarization-multiplexed link using a data-carrying beacon on a separate wavelength, *Opt. Lett.* 40, 2249–2252 .
- [24] **Sasiela, R.J.** (2007), *Electromagnetic wave propagation in turbulence*, 2nd Edition, SPIE.
- [25] **Kolmogorov, A. N.** (1941), The local structure of turbulence in incompressible viscous fluid for very large Reynolds numbers, *Doklady Akademii Nauk SSSR*, Vol. 30, No. 4, 301–305.
- [26] **ZENG, J.** et. al. (2019), Spiral spectrum of a Laguerre-Gaussian beam propagating in anisotropic non-Kolmogorov turbulent atmosphere along horizontal path, 27, 18, *Optics Express*, 25342.

- [27] **Khalighi, M.A.** (2009), Fading Reduction by Aperture Averaging and Spatial Diversity in Optical Wireless Systems, *J. OPT. COMMUN. NETW.* 1, 6.
- [28] **Liu, X.** et al. (2013), “Experimental demonstration of vortex phase-induced reduction in scintillation of a partially coherent beam,” *Opt. Lett.* 38 5323–5326.
- [29] **Liu, X. and Pu, J.** (2011), Investigation on the scintillation reduction of elliptical vortex beams propagating in atmospheric turbulence, *Opt. Express* 19, 26444-26450.
- [30] **Chen, Z.** et al. (2012), Experimental investigation on the scintillation index of vortex beams propagating in simulated atmospheric turbulence, *Appl. Phys. B* 107, 469–472.
- [31] **Berman, G.P.** et. al. (2011), Scintillation reduction for combined Gaussian-vortex beam propagating through turbulent atmosphere, *Proceedings of SPIE, Bellingham, Atmospheric and Oceanic Propagation of Electromagnetic Waves V*, 7924:79240G-1–13.
- [32] **Eyyuboğlu, H.T.** (2016), Scintillation behaviour of vortex beams in strong turbulence region, *J. Mod. Opt.* 63, 2374–2381.
- [33] **Wang, X. and Song, Y.** (2018), Transmission characteristics of Bessel–Gaussian vortex beams propagating along both longitudinal and transverse directions in a subway tunnel, *Opt. Eng.* 57(2), 024105-1-9.
- [34] **Li, J.** et. al. (2016), Analysis to beam quality of partially coherent flat-topped vortex beams propagating through atmospheric turbulence, *Optik* 127, 11342–11348.
- [35] **Liua, D.** et al. (2016), Average intensity properties of flat-topped vortex hollow beam propagating through oceanic turbulence, *Optik* 127, 6961–6969.
- [36] **Gbur, G. and Tyson, R. K.** (2008), “Vortex beam propagation through atmospheric turbulence and topological charge conservation,” *J. Opt. Soc. Am. A* 25(1).
- [37] **Liu, D.** et. al. (2015), Evolution properties of partially coherent flat topped vortex hollow beam in oceanic turbulence, *Applied Optics* 54(35), 10510-10516.
- [38] **Liu, D.** et. al. (2016), Intensity properties of flat-topped vortex hollow beams propagating in atmospheric turbulence, *Optik* 127, 9386–9393.
- [39] **Zhu, K.** et. al. (2008), Propagation of Bessel-Gaussian beams with optical vortices in turbulent atmosphere, 16, 26, *Optics Express*, 21315-21320.

- [40] **Cheng, M.** et. al. (2016), Propagation properties of an optical vortex carried by a Bessel–Gaussian beam in anisotropic turbulence, 33, 8, Journal of the Optical Society of America A, 1442-1450.
- [41] **Zhu, K.** et. al. (2012), Study on the propagation parameters of Bessel–Gaussian beams carrying optical vortices through atmospheric turbulence, 29, 3, J. Opt. Soc. Am. A 251-257.
- [42] **Lee, A.L. and Omatsu, T.** (2017) Direct Generation of Vortex Laser Beams and Their Non-Linear Wavelength Conversion, Chapter, <http://dx.doi.org/10.5772/66425>.
- [43] **Veysi, M.** et. al. (2018), Revisiting Orbital Angular Momentum Beams, IEEE Antennas and Propagation Magazine 1045-9243.
- [44] **Eyyuboğlu, H.T.** (2013), Scintillation analysis of hypergeometric Gaussian beam via phase screen method,” Optics Communications 309, 103–107.
- [45] **Eyyuboğlu, H.T.** et. al. (2013), Scintillation analysis of truncated Bessel beams via numerical turbulence propagation simulation, Applied Optics 52(33), 8032-8039.
- [46] **Eyyuboğlu, H.T.** (2013), Estimation of aperture averaged scintillations in weak turbulence regime for annular, sinusoidal and hyperbolic Gaussian beams using random phase screen, Opt. Laser Technol. 52, 96–102.
- [47] **Eyyuboğlu, H.T.** (2013), Scintillation analysis of hypergeometric Gaussian beam via phase screen method, Opt. Commun. 309, 103–107.
- [48] **Eyyuboğlu, H.T.** et. al. (2013), Scintillation analysis of truncated Bessel beams via numerical turbulence propagation simulation, Appl. Opt. 52, 8032-8039.
- [49] **Chatterjee, M.R.** et. al. (2018), Secure free-space communication, turbulence mitigation, and other applications using acousto-optic chaos, Appl. Opt. 57(10), C1-C13.
- [50] **Mohamed, A. and Chatterjee, M.R.,** (2019), Image intensity recovery with mitigation in the presence of gamma–gamma atmospheric turbulence using encrypted chaos, Opt. Eng. 58(3), 036110.
- [51] **Rao, R.** (2008), Statistics of the fractal structure and phase singularity of a plane light wave propagation in atmospheric turbulence, Appl. Opt. 47, 269–276.
- [52] **Schmidt, J.D.** (2010), Numerical simulation of optical wave propagation with examples in MATLAB, SPIE Press: Washington, DC, Chapters 7, 8 and 9.

- [53] **Zhai, H.** et. al. (2015), Fractal phase screen generation algorithm for atmospheric turbulence, 54, 13, Applied Optics.
- [54] **Eyyuboğlu, H.T.** et. al. (2006), Flat topped beams and their characteristics in turbulent media, 14, 10 Optics Express.
- [55] **Dickey, F.M. and Holswade, S.C.** (2000), Laser beam shaping: theory and techniques, Marcel Dekker, New York.
- [56] **Baykal, Y and Eyyuboğlu, H.T.** (2006), Scintillation index of flat-topped Gaussian beams, 45, 16 Applied Optics.
- [57] **Vasilyeu, R.** et. al. (2009), “Generating superpositions of higher-order Bessel beams,” Opt. Express 17, 23389–23395.
- [58] **Cheng, M.** et. al. (2016), Channel capacity of the OAM based free-space optical communication links with Bessel-Gauss beams in turbulent ocean, IEEE Photon. J. 8, 7901411.
- [59] **Eyyuboğlu, H.T.** et. al. (2006), “Convergence of general beams into Gaussian intensity profiles after propagation in turbulent atmosphere,” Optics Communications 265, 399–405.
- [60] **Wang, L.G. and Zheng, W.W.** (2009), The effect of atmospheric turbulence on the propagation properties of optical vortices formed by using coherent laser beam arrays, J. Opt. A: Pure Appl. Opt. 11
- [61] **Eyyuboğlu, H.T.** (2015), Aperture averaged scintillation of fully and partially coherent Gaussian, annular Gaussian, flat topped and dark hollow beams, Opt. Commun. 339, 141–147
- [62] **Elmabruk, K. and Eyyuboğlu, H.T.** (2019), Analysis of Flat-Topped Gaussian Vortex Beam Scintillation Properties in Atmospheric Turbulence”. Optical Engineering. 58(6).
- [63] **Dravins, D.** et al. (1997), Atmospheric intensity scintillation of stars, I. statistical distributions and temporal properties, Publications of the Astronomical Society of the Pacific 109, 173-207.

CURRICULUM VITAE

PERSONAL INFORMATION

Name Surname: Kholoud ELMABRUK

Date of Birth: 30/12/1984

E-mail: kholoudelmabruk@gmail.com

EDUCATION

High School: (1998-2001) Al qodus High School, Gharian/Libya.

Bachelor: (2001-2006) Electrical and electronic engineering dep. "Communication", Aljabal Algarbi University, Gharian/Libya, (79.22/100).

Master Degree: (2010-2012) Communication and electronic engineering dep./ Çankaya University, Ankara/Turkey, (3.81/4.00).

Ph.D. Degree: (2013-2019) Electrical and Electronics Engineering Department/ Ankara Yıldırım Beyazıt University, Ankara/Turkey, (3.86/4.00).

WORK EXPERIENCE

- (2008-2009): research assistance at Aljabal Algarbi University, Garian/ Libya.

Courses taught:

- Basics of electronic circuits.

- Analog electronic circuits.
 - Signals and systems.
- 2006-2007: trainee at OXY petroleum ltd, Tripoli/ Libya.

PUBLICATIONS:

Journal Publications - Peer-review:

- ***Kholoud Elmabruk***, Halil Eyyuboglu, “Analysis of Flat-Topped Gaussian Vortex Beam Scintillation Properties in Atmospheric Turbulence”. *Optical Engineering*. 58(6). 2019
- ***Kholoud Elmabruk***, Kazim Demir, Asaf Bahzit Sahin, Hakan Altan, Mehmet Unlu, “Time-Domain Characterization of the Radiation Pattern of the Terahertz Photoconductive Antennas”. *Journal of Infrared, Millimeter, and Terahertz Waves*. DOI: 10.1007/s10762-019-00588-y. 2019
- Ali Haider, Petro Deminskyi, Mehmet Yilmaz, ***Kholoud Elmabruk***, Ibrahim Yilmaz, Necmi Biyikli, “Long-range ordered vertical III-nitride nanocylinder arrays via plasma-assisted atomic layer deposition”. *J. Mater. Chem. C*. (6) 6471-6482. 2018

Conference Proceedings:

- ***Kholoud Elmabruk***, Kazim Demir, Asaf Bahzit Sahin, Hakan Altan, Mehmet Unlu, “Radiation Pattern Characterization of Terahertz Photoconductive Antennas Using Time-Domain Spectroscopy System”. 2018 IEEE International Symposium on Antennas and Propagation and USNC-URSI Radio Science Meeting, Boston, MA, USA. 8-13. (2018).
- Ali Haider, Petro Deminskyi, ***Kholoud Elmabruk***, Sevde Altuntas, Ibrahim Yilmaz, Fatih Buyukserin, Necmi Biyikli, “Low-Temperature Conformal Growth of Ordered III-nitride and Metal-Oxide Hollow Nanocylinder Arrays for Optoelectronics and Photocatalytic”, MRS Fall Meeting, Boston, Massachusetts, 27 November – 2 December (2016).
- Ibrahim Yilmaz, ***Kholoud Elmabruk***, Ali Haider, Sevde Altuntas, Fatih Buyukserin, Necmi Biyikli, “Temperature-dependent photoluminescence characteristics of plasmaassisted ALD-grown ordered GaN nanostructures on

Si substrates”, 16th International Conference on Atomic Layer Deposition (ALD 2016), Dublin, Ireland, 24 – 27 July (2016).

- Ali Haider, Cagla Ozgit-Akgun, ***Kholoud Elmabruk***, Ibrahim Yilmaz, Necmi Biyikli, “Template Assisted Growth of GaN Nanostructures by Hollow Cathode Plasma-assisted Atomic Layer Deposition”, 15th International Conference on Atomic Layer Deposition (ALD 2015), Portland, OR. 28 June – 2 July (2015)

Projects:

- “Beam steering, frequency reconfigurable terahertz photomixer array using nano-actuators”. Funded by: EU H2020 Marie Skłodowska Curie Program, Reintegration (RI) Grant.
- “Development of frequency reconfigurable, wideband, high radiation resistance photomixers and photoconductive antennas for terahertz frequencies (114E089)”. Funded by: TUBITAK (3501).

Skills:

Languages:

- Arabic “first language”
- English “advanced”
- Turkish “intermediate”

Computer:

- ICDL “International computer driving license”
- MATLAB
- Origin
- CST
- HFSS